

Trustworthy Reinforcement Learning for Quadrotor UAV Tracking Control Systems

Yanran Wang, David Boyle

Abstract—Simultaneously accurate and reliable tracking control for quadrotors in complex dynamic environments is challenging. As aerodynamics derived from drag forces and moment variations are chaotic and difficult to precisely identify, most current quadrotor tracking systems treat them as simple ‘disturbances’ in conventional control approaches. We propose a novel, interpretable trajectory tracker integrating a Distributional Reinforcement Learning disturbance estimator for unknown aerodynamic effects with a Stochastic Model Predictive Controller (SMPC). The proposed estimator ‘Constrained Distributional Reinforced disturbance estimator’ (ConsDRED) accurately identifies uncertainties between true and estimated values of aerodynamic effects. Simplified Affine Disturbance Feedback is used for control parameterization to guarantee convexity, which we integrate with a SMPC. We theoretically guarantee that ConsDRED achieves an optimal global convergence rate, and sublinear rates if constraints are violated with certain error decreases as neural network dimensions increase. To demonstrate practicality, we show convergent training in simulation and real-world experiments, and empirically verify that ConsDRED is less sensitive to hyperparameter settings compared with canonical constrained RL approaches. We demonstrate our system improves accumulative tracking errors by at least 70% compared with the recent art. Importantly, the proposed framework, ConsDRED-SMPC, balances the tradeoff between pursuing high performance and obeying conservative constraints for practical implementations¹.

Index Terms—Interpretable reinforcement learning, robot learning, unmanned aerial vehicles.

I. INTRODUCTION

ACCURATE trajectory tracking for autonomous Unmanned Aerial Vehicles (UAVs), such as quadrotors, is necessary for maintaining autonomy. Although industrial applications of autonomous UAVs [1], [2] have attracted much attention in recent years, precisely and reliably tracking high-speed and high-acceleration UAV trajectories is an extremely challenging control problem, particularly in unknown environments with unpredictable aerodynamic forces.

To achieve safe, precise and reliable quadrotor trajectory tracking, two main problems that need to be solved: How to achieve accurate and trustworthy estimation (or modelling) of the variable aerodynamic effects using limited onboard computational resources? And; How can the whole control framework be integrated with the aerodynamic effect estimation to track trajectory references precisely and reliably?

Previous work has shown that the primary source of quadrotor uncertainties are aerodynamic effects deriving from drag

forces and moment variations caused by the rotors and the fuselage [3]. Wind tunnel experiments shows that aggressive maneuvers at high speed, e.g., greater than 5 ms^{-1} , introduce large positional and attitude tracking errors [4]. Although modelling aerodynamic effects precisely in static environments like no-gust indoor areas, data-driven approaches - e.g., Gaussian Processes (GP) [3], [5] and neural networks [6], [7] - perform poorly in complex environments. The main reason is the generalization ability: their training datasets, collected from simulated platforms or real-world historical records, do not fully describe the complex environments.

Reinforcement Learning (RL) is able to solve the complex and changeable sequential decision-making process [8] with iteratively interactive learning. The key challenge of most existing RL approaches [9] is: policy optimization relies on nebulous black/grey-boxes, where deep neural networks are poorly explainable and the global convergence is historically unstable [10], [11], [12]. These challenges mean that traditional RL results are often irreproducible [13] - i.e., the same hyperparameter setting yields a huge discrepancy between the stated and reproduced results. Because of this uncontrollable and non-interpretable convergence process, industrial applications of RL are often unacceptable, particularly in safety-critical applications such as autonomous robots [5], [14] and financial services [15].

To address the stated issues, we propose **Constrained Distributional Reinforced-Disturbance-estimation** for Stochastic MPC (ConsDRED-SMPC), a systematic, trustworthy and feasible quadrotor trajectory tracking framework for use under high variance aerodynamic effects. The details are as follows:

- 1) **Aerodynamic Disturbance Estimator**: a Constrained Distributional Reinforced-disturbance-estimator (ConsDRED; Algorithm 1), is proposed for aerodynamic disturbance estimation. This estimation relies on wind estimation obtained from VID-Fusion [16] (see Fig. 1 for more details). ConsDRED builds upon prior QR-DQN [17] and QUOTA [18] insofar as ConsDRED is a quantile-approximated constrained distributional RL which uses a set of quantiles to approximate the full value distribution in a Constrained RL (CRL, also known as safe RL) framework. Section V-A shows that ConsDRED can not only guarantee the convergence (i.e., *Theorem 1*), but also achieve at least an $\Theta(1/\sqrt{K})$ convergence rate (*Proposition 4*) to local policy evaluation (i.e., the distributional temporal difference (TD) learning defined in Equation 6) and at least an $\Theta(1/\sqrt{T})$ convergence rate (*Theorem 2*) to global policy optimization, respectively.

¹Our code and all research artefacts will be made openly available upon acceptance of our manuscript for publication. Video figures in support are also available: <https://github.com/Alex-yanranwang/ConsDRED-SMPC>.

- 2) Trajectory Tracker: Similar to [19], a Simplified Affine Disturbance Feedback (SADF) is used for control parameterization in SMPC (Algorithm 2), where the convexity can be guaranteed in this process [20] and computational complexity can be reduced. Different from prior work assuming zero mean disturbance, we consider the control performance and stability under non-zero-mean disturbance. We use an Input-to-State Stability (ISS) [21] property to find conditions that imply stability and convergence of the tracker.
- 3) The ConsDRED-SMPC framework is proposed to track quadrotor trajectory accurately under high variance aerodynamic effects. The overall control framework is shown in Fig. 1. In Section V-B, the closed-loop stability of ConsDRED-SMPC is demonstrated under the Lipschitz Lyapunov function [22].

Our contributions can be summarized as follows:

- 1) ConsDRED, a constrained distributional RL with quantile approximation that can sufficiently estimate variable aerodynamic disturbances. In the cases tested, we show that ConsDRED outperforms the state-of-the-art CRL, such as CRPO [12], and prior Distributional RL approaches, such as QuaDRED [23]. More importantly, ConsDRED achieves at least an $\Theta(1/\sqrt{T})$ global convergence rate, which offers an interpretable and trustworthy guarantee to the practical training implementation.
- 2) The integration of a trajectory tracker with an aerodynamic disturbance estimator, a quadrotor trajectory tracking framework that integrates ConsDRED into a stochastic optimal control problem.
- 3) Convergence and stability guarantees: mathematical proofs are provided for the convergence rate of constrained distributional-RL-based estimator, and the closed-loop stability of stochastic-MPC-based tracker with consideration of non-zero-mean and bounded disturbances.

II. MOTIVATION AND RELATED WORK

A. Estimation of Aerodynamic Effects

Aerodynamics explains how the air moves around things [28], where prominent aerodynamic disturbances appear at flight speeds of 5 ms^{-1} in wind tunnel experiments [4]. These effects acting on quadrotors are chaotic and hard to model directly, as they are generated from a combination of the individual propellers and airframe [29], turbulent effects caused by rotor-rotor and airframe-rotor interactions [30], and the propagation of other turbulence [31].

Most current approaches to quadrotor trajectory tracking treat aerodynamic effects as simple external disturbances, and do not account for higher-order effects or attempt to deviate from a determined plan [32], [33], [34]. While these solutions are efficient and feasible for lightweight on-board computers, aggressive flight at high speed (e.g., $\geq 5 \text{ ms}^{-1}$) introduce large tracking errors [4]. Recent data-driven approaches, such as GPs [3], [5] and neural networks [6] combined with Model Predictive Control (MPC), show accurate modelling

of aerodynamic effects. However, the nonparametric nature of GP causes them perform poorly in complex environments, leading to escalating computational demands as the training set size increases [35], particularly when large datasets contain drastic changes in wind speed and heading. In these instances, learning-based (neural networks) approaches perform better than GP-based approaches [36], [37], [38]. Achieving adaptability and robustness in complex environments is still challenging, however, primarily because training datasets are static and most do not completely identify the complex environmental dynamics [35].

B. Reinforcement Learning in real physical systems: insights from Distributional and Constrained perspectives

Simulation to reality in reinforcement learning: In real-world scenarios, the inherent challenges posed by observation dimensionality, task complexity, or exploration difficulty make the utilization of synthetic experience a nature attraction for practical implementation of RL [39]. Simulation to Reality (Sim-to-Real) RL methods [40], [41], [42] leverage simulation platforms to efficiently train policies within virtual replicas of the intended environment. Subsequently, these trained policies are transferred to the real-world domain. To overcome the Sim-to-Real gap, approaches proposed in [3], [43] enhance the accuracy of model identification, while domain randomization techniques, as employed in [44], [45], contribute to improving learning generalization.

Distributional representation in reinforcement learning: In comparison to existing data-driven approaches, RL, an interactive learning process, can learn complex and changeable disturbances, i.e., the errors between true and estimated values, using much less model information [8]. However, to maximize the accumulated rewards, policy optimization biases toward actions with high variance value estimates, since some of these values will be overestimated by random chance [46]. In risk-sensitive applications such as real-world autonomous navigation these actions should be avoided. Recent work on distributional RL [47] proposes to approximate and parameterize the entire distribution of future rewards, instead of the expected value. Distributional RL algorithms have been shown to achieve promising results on continuous control domains [48]. In principle, more complete and richer value-distribution information are provided to enable a more stable learning process [47]. Previous distributional RL algorithms parameterize the policy value distribution in different ways, including canonical return atoms [47], the expectiles [49], the moments [50], and the quantiles [17], [18]. The quantile approach is especially suitable for autonomous UAV trajectory tracking [23] due to its risk-sensitive policy optimization.

Constrained reinforcement learning addressed through primal-dual approaches: In the setting above, the agent is allowed to explore the entire state and action space without any constraints, where one issue is [51]: **how can we guarantee safety when we apply RL for real-world applications?** In CRL, however, the space is explored under safe constraints, where the goal of policy optimization is to maximize the rewards whilst satisfying the certain safe constraints [11]. Two

TABLE I: Comparison of Tracking Control Methods for Quadrotor UAVs

Methods	Algorithm	Safe and trustworthy consideration				
		Non-conservative	Unknown structure uncertainties	Safety constraints	Combining with model-based control	Formal stability
Robust control	Abdelmoet et. al., 2016 [24]	✗	✓	✓	✓	✓
	Raffo et. al., 2016 [25]	✗	✓	✓	✓	✓
	Nguyen et. al., 2021 [14]	✗	✓	✓	✓	✗
Adaptive control	Zhang et. al., 2018 [26]	✓	✗	✓	✓	✓
	Zhang et. al., 2021 [8]	✓	✗	✓	✓	✓
Adaptive dynamic programming	Dou et. al., 2021 [27]	✓	✓	✗	✗	✓
Data-driven approach	Torrente et. al., 2021 [3]	✓	✗	✗	✓	✗
	Wang et. al., 2022 [5]	✓	✓	✗	✓	✗
	Spielberg et. al., 2021 [6]	✓	✓	✗	✓	✗
Our method		✓	✓	✓	✓	✓

main categories of CRL solutions are the **primal** and **primal-dual** approaches. The primal-dual approaches, combining the value function with a sum of constraints weighted by corresponding Lagrange multipliers, are frequently adopted in CRL, e.g., the well-known RCPO [52], CPPO [53] and PPO [54]. Theoretically, in these primal-dual methods, [52] gives an asymptotic convergence guarantee and [54] achieves a regret bound for linear constrained MDP. However, the primal-dual approach can be severely sensitive to these hyperparameters: the tuning of the learning rates and threshold of the dual Lagrange multipliers. This means that the primal-dual approach is determined by the initialization of those hyperparameters, and thus acquires additional costs in hyperparameter tuning [52]. On the other side, the primal approach [55], [56], [12] designs the objective functions diversely without the dual Lagrange variables, and receives much less attention than the primal-dual approach. CRPO [12] proposes the first primal algorithm with a provable convergence guarantee. However, it is only established on simpler 2-layer neural networks, which is impractical for large-scale search space, i.e., extension to multi-layer neural networks.

To address the concerns above, the three perspectives of RL research have emerged. We use a distributional RL based on quantile approximation for modelling the state-action distribution, incorporating Sim-to-Real RL training (detailed setting provided in Section VI-A). Then we employ a primal algorithm for constrained policy optimization. Compared with [23], our proposed ConsDRED guarantees $\Theta(1/\sqrt{T})$ convergence rate in both local policy evaluation and global policy optimization. Building on [12], our work extends the convergence guarantees to (multi) H -layer neural networks (see *Proposition 4* and *Theorem 2*) for practical implementation. Our numerical experiments also demonstrate that ConsDRED achieves at least 39% and 12% improvement of tracking errors than CRPO [12] in the simulated and real-world scenarios, respectively (see Section VI-B).

C. Tracking Control Framework under Disturbances

Quadrotor UAV tracking control for uncertain systems can be categorized into four main approaches: **1)** Robust control adopts a "worst-case" formulation to handle bounded uncertainties and disturbances [57], [58]. However, in real-

world scenarios where uncertainties are present, this worst-case design can lead to suboptimal and overly conservative control actions [59], [60]. **2)** Adaptive control is capable of dealing with varying uncertainties with unknown boundaries, but it assumes that uncertainties are linearly parameterized with known structure and unknown parameters [8], [26]. **3)** Adaptive Dynamic Programming (ADP) belongs to a specific class of RL algorithms that combine dynamic programming and RL principles. ADP emphasizes updating value functions or policies using dynamic programming principles, making it suitable for handling large state and action spaces. However, ADP also has some weaknesses in quadrotor control [27], which typically rely on accurate models for effective convergence, and uncertainty in the model can impact the quality of the learned policy. **4)** Data-driven approaches, such as Gaussian Processes (GP) [3], [5] and neural networks [6], efficiently model aerodynamic effects in static environments like indoor areas without gusts. However, these methods perform poorly in complex environments like forests due to their limited generalization capabilities. A concise comparison between existing methods and our proposed method is presented in Table I.

Robust MPC for tracking control of uncertain systems like quadrotors [38], [57], [61] is rapidly developing thanks to advances in hardware and algorithm efficiency [14]. To avoid the conservatism of the worst case design, Stochastic MPC (SMPC) [62], [63] uses the probabilistic descriptions, such as stochastic constraints (also called chance constraints), to predict probability distributions of system states within acceptable levels of risk in the receding-horizon optimization [64].

The core challenges for SMPC include: 1) optimizing the feedback control laws over arbitrary nonlinear functions [65]; 2) the chance constraints are non-convex and intractable [60], [19]; and 3) the computational complexity will grow dramatically as more uncertainties are added. To address the first challenge, one solution is to use affine parameterization of the control policy over finite horizons. However, this approach cannot guarantee convexity, i.e., the second challenge, where the policy set may still be convex [20]. Another solution is an Affine Disturbance Feedback (ADF) control parameterization, proposed in [66]. This ADF control parameterization can

address the first two challenges, which are optimizing the dynamic function and guaranteeing the decision variables to be convex, respectively. However, the main weakness is that the computational complexity grows quadratically with the prediction horizon, i.e., the third challenge. To overcome this difficulty, a Simplified Affine Disturbance Feedback (SADF) proposed in [19], where the SADF is equivalent to ADF but a finite-horizon optimization can be computed more efficiently using CasADi [67], a nonlinear MPC solver. [19] achieves good results by implementing SADF with zero-mean disturbance, however it is unclear how the SADF would perform on systems with non-zero-mean disturbances, such as a quadrotor.

III. PROBLEM FORMULATION

A. Dynamic Model of Quadrotors

A quadrotor dynamic model has six Degrees of Freedom (DoF), i.e., three linear motions and three angular motions [3]. Let $\mathbf{x} = [\mathbf{P}_{WB}, \mathbf{V}_{WB}, \mathbf{q}_{WB}, \boldsymbol{\omega}_B]^T \in \mathbb{X} \subseteq \mathbb{R}^n$, $\mathbf{u} = [\mathbf{c}, \boldsymbol{\tau}_B]^T$ and \mathbf{e}_f be the state, control input and aerodynamic effect, respectively. \mathbf{P}_{WB} , \mathbf{V}_{WB} and \mathbf{q}_{WB} are the position, linear velocity and orientation of the quadrotor, and $\boldsymbol{\omega}_B$ is the angular velocity [5]. \mathbf{c} and $\boldsymbol{\tau}_B$ are the collective thrust, defined as $\mathbf{c} = [0, 0, \sum T_i]^T$, and the body torque, defined in (Equation 2 in) [3], respectively. T_i is the thrust of the i -th ($i \in [0, 3]$) motor. We consider the continuous-time nominal model of quadrotors defined in Equation 1:

$$\begin{aligned} \dot{\mathbf{P}}_{WB} &= \mathbf{V}_{WB} & \dot{\mathbf{V}}_{WB} &= \mathbf{g}_W + \frac{1}{m}(\mathbf{q}_{WB} \odot \mathbf{c} + \mathbf{e}_f) \\ \dot{\mathbf{q}}_{WB} &= \frac{1}{2}\Lambda(\boldsymbol{\omega}_B)\mathbf{q}_{WB} & \dot{\boldsymbol{\omega}}_B &= \mathbf{J}^{-1}(\boldsymbol{\tau}_B - \boldsymbol{\omega} \times \mathbf{J}\boldsymbol{\omega}_B) \end{aligned} \quad (1)$$

where $\mathbf{g}_W = [0, 0, -\mathbf{g}_w]^T$. The operator \odot denotes a rotation of the vector by the quaternion. The skewsymmetric matrix $\Lambda(\boldsymbol{\omega})$ is defined in [5].

We discretize and linearize [66] Equation 1 for MPC over a finite horizon N :

$$\mathbf{x}_t = \mathbf{A}\mathbf{x}_{0|t} + \mathbf{B}\mathbf{u}_t + \mathbf{G}\mathbf{w}_t \quad (2)$$

where $\mathbf{x}_t = [x_{0|t}^T, x_{1|t}^T, \dots, x_{N|t}^T]^T$ and $\mathbf{u}_t = [u_{0|t}^T, u_{1|t}^T, \dots, u_{N|t}^T]^T$ are the sequential discrete-time states and inputs of the quadrotor nominal model. $\mathbf{w}_t = [w_{0|t}^T, w_{1|t}^T, \dots, w_{N|t}^T]^T$, a sequential stochastic disturbance (over a horizon of N) caused by aerodynamic effects, inaccuracy in VID-Fusion [16], dynamic discrepancy of nominal model and linearization error, equals to the action output of ConsDRED (an aerodynamic disturbance estimator) proposed in Section IV-A). \mathbf{A} , \mathbf{B} and \mathbf{G} are matrices defined in [19].

B. Constrained Distributional Markov Decision Process

We consider a Constrained Distributional Markov Decision Process (CDMDP), combining a discounted Constrained Markov Decision Process (CMDP) [68] and a distributional Bellman equation [69].

The CMDP is formulated as a discounted Markov Decision Process (MDP) with additional constrained objectives, i.e., a tuple $\langle S, A, P, R, g, \gamma \rangle$, where S is a finite set of states $\{s\}$,

A is a finite set of actions $\{a\}$, $P : S \times A \rightarrow S$ is a finite set of transition probabilities $\{p\}$, $R : S \times A \times S \rightarrow \mathbb{R}$ is a finite set of bounded immediate rewards $\{r\}$, g is a unity function where the agent is constrained into a ‘safe’ state, and $\gamma \in [0, 1]$ is the discount rate. A stationary policy π maps one state s to one action a . The following constrained problem is presented as a CMDP:

$$\max_{\pi} \mathcal{J}_r(\pi), \quad \text{s.t.} \quad \mathcal{J}_g^i(\pi) \leq \mathbf{b}_i, \quad i = 1, \dots, p \quad (3)$$

where $\mathcal{J}_r(\pi) := \mathbb{E}[\sum_{t=0}^{\infty} \gamma^t r(s_t, a_t) | \pi, s_0 = s]$ and $\mathcal{J}_g^i(\pi) := \mathbb{E}[\sum_{t=0}^{\infty} \gamma^t g^i(s_t, a_t) | \pi, s_0 = s]$ are the value function associated with the reward r and the utility g , respectively, and where $s_{t+1} \sim p(\cdot | s_t, a_t)$ and $a_t \sim \pi(\cdot | s_t)$ at each time step, t .

The distributional Bellman equation [47], the aim of which is different from traditional RL, maximizes the expectation of value-action function Q . In the policy evaluation setting, given a deterministic policy π , the state-action distribution Z^π and the Bellman operator \mathcal{T}^π are defined as [47], [17]:

$$\mathcal{T}^\pi Z(s, a) \stackrel{D}{=} R(s, a) + \gamma Z(S', A') \quad (4)$$

where the state $\mathbf{s} = [\mathbf{P}_{WB}, \mathbf{V}_{WB}, \mathbf{q}_{WB}, \boldsymbol{\omega}_B, \mathbf{e}_f]^T \in S$, the action $\mathbf{a} = \mathbf{u} \in A$, and S' and A' are the sets of states and actions sampled at the next time step.

The following assumptions are made:

Assumption 1: Matrix \mathbf{G} is column full rank.

Assumption 2: The aerodynamic effect \mathbf{e}_{fk} is available with no delay at each sampling timestamp.

Proposition 1: There exists a control law \mathbf{u}_b that ensures the nominal model $\mathbf{f}(\mathbf{x}_k, \mathbf{u}_k, \mathbf{e}_{fk})$ is ISS if the stochastic disturbance \mathbf{w}_t is an independent and identically distributed (i.i.d.) zero-mean distribution, i.e., $\mathbb{E}(\mathbf{w}_k) = 0$.

Proof: Based on *Assumption 2*, the nominal model $\mathbf{f}(\mathbf{x}_k, \mathbf{u}_k, \mathbf{e}_{fk})$ is seen as $\mathbf{f}(\mathbf{x}_k, \mathbf{u}'_k)$, in which the aerodynamic force \mathbf{e}_{fk} is a constant term. Then, based on [21], [65], [66], $\mathbf{f}(\mathbf{x}_k, \mathbf{u}_k)$ is an ISS-Lyapunov function. ■

IV. CONSDRED-SMPC

In this section, we present the proposed ConsDRED-SMPC control framework. Traditional non-interacted methods, e.g., GP [3] and RDRv [4], are insufficient for quadrotor dynamic disturbance estimation. This work addresses the limitation, and proposes a novel and feasible disturbance estimation with continuous environmental interactions for variable winds.

A. Constrained Distributional Reinforced Estimation

Policy Evaluation: to perform the policy evaluation in Equation 4 and Algorithm 1 (Line 5), we guarantee the contraction of the Bellman operator \mathcal{T}^π over the Wasserstein Metric (see Equation 5) and then adopt Wasserstein distance to obtain the distance between the target $\mathcal{T}^\pi Z$ and the prediction Z .

The Wasserstein Metric, also known as the Mallows metric, is a true probability metric with no disjoint support issues. A contraction is proved in [17] over the Wasserstein Metric:

$$\bar{d}_\infty(\Pi_{W_1} \mathcal{T}^\pi Z_1, \Pi_{W_1} \mathcal{T}^\pi Z_2) \leq \bar{d}_\infty(Z_1, Z_2) \quad (5)$$

where W_p , $p \in [1, \infty]$ denotes the p -Wasserstein distance. $\bar{d}_p := \sup W_p(Z_1, Z_2)$ denotes the maximal form of the p -Wasserstein metrics. T , as defined in Equation 7 below, is a distributional Bellman optimality operator, and Π_{W_1} is a quantile approximation under the minimal 1-Wasserstein distance W_1 .

Based on the above contraction guarantees, we employ TD learning to estimate the state-action value distribution Z , where in each iteration we propose:

$$\begin{aligned} \zeta_{k+1}^i(s, a) &= \zeta_k^i(s, a) + l_{td} \Delta_k^i = \zeta_k^i(s, a) + l_{td} \times \\ &\bar{d}_\infty(\Pi_{W_1} \mathcal{T}^\pi(h_i(s, a, s') + \gamma \zeta_k^i(s')), \Pi_{W_1} \mathcal{T}^\pi \zeta_k^i(s, a)) \end{aligned} \quad (6)$$

where $\zeta_k^i \in S \times A$ is the estimated distribution of the state-action distribution Z in the k -th TD-learning-iteration for all $i = 0, \dots, p$, and l_{td} is the TD learning rate. $h_i : S \times A \times S \rightarrow \mathbb{R}$ maps (s, a, s') to a *Real Number*, of which the definition is $h_i = r$ when $i = 0$; and $h_i = g^i$ when $i \in [1, p]$. The distributional TD error Δ_k^i in Equation 6 is calculated by $\bar{d}_\infty(\Pi_{W_1} \mathcal{T}^\pi(h_i(s, a, s') + \gamma \zeta_k^i(s')), \Pi_{W_1} \mathcal{T}^\pi \zeta_k^i(s, a))$.

It has been shown in [17], [70] that the quantile approximation of the Bellman operator $\Pi_{W_1} \mathcal{T}$ is a contraction over the maximal form of the Wasserstein distance \bar{d}_∞ . Therefore, after performing K_{td} iterations, ζ_k^i will be contracted and converge to a fixed point $\zeta_*^i \in S \times A$, and then we let $Z_t^i(s, a) = \zeta_{K_{td}}^i(s, a), \forall (s, a) \in S \times A$ and $\forall i \in [0, p]$.

Constraint Estimation: the constraint function $\mathcal{J}_g^i(\pi)$ is approximated via weighted utility function $g^i(s_t, a_t)$, i.e., $\bar{\mathcal{J}}_g^i(\pi) = \mathbb{E}[\sum_{t=0}^{\infty} \gamma^t g^i(s_t, a_t) | \pi, s_0 = s] = \mathbb{E}[\zeta_{K_{td}}^i(s, a)], \forall i \in$

$[1, p]$. Then we have $|\bar{\mathcal{J}}_g^i(\pi) - \mathcal{J}_g^i(\pi)| = |\mathbb{E}[\zeta_{K_{td}}^i(s, a)] - \mathbb{E}[g^i(s, a)]| \leq \|\zeta_{K_{td}}^i(s, a) - g^i(s, a)\|, \forall i \in [1, p]$. Therefore, the error of the constraint estimation is upper bounded [12], and the constraint estimation $\bar{\mathcal{J}}_g^i(\pi)$ is precise when the utility estimation $\zeta_{K_{td}}^i(s, a)$ is precise. Concretely, when the utility outputs are in *Real Space* (i.e., $g^i \in \mathbb{R}$), the Wasserstein distance \bar{d}_∞ (Equation 5) will be degenerated to the canonical Euclidean distance whilst the distributional TD learning (Equation 6) will be degenerated to the traditional TD learning proposed in [71], [72].

Policy Improvement: In control setting, a distributional *Bellman optimality operator* \mathcal{T} with quantile approximation is proposed in [17]:

$$\mathcal{T}Z(s, a) \stackrel{D}{=} R(s, a) + \gamma Z(s', \argmax_{a', R} \mathbb{E}[Z(s', a')]) \quad (7)$$

where $\hat{Z} := \frac{1}{N} \sum_{i=1}^N \delta_{q_i(s, a)} \in Z_Q$ is a quantile distribution mapping one state-action pair (s, a) to a uniform probability distribution supported on q_i . Z_Q is the space of quantile distribution within N supporting quantiles. δ_z denotes a Dirac with $z \in \mathbb{R}$. The state-action value Q is then approximated by $Q_{j|K} \stackrel{D}{=} \frac{1}{K} \sum_{k=(j-1)K+1}^{(j-1)K+K} q_k(s, a)$. These quantile approximations, i.e., $\{q_i\}$, are operated based on Quantile Huber Loss.

We propose the ConsDRED (Algorithm 1) to solve the CDMDP problem in Equation 8. The goal of ConsDRED lies in maximizing the unconstrained value function (i.e., $\mathcal{J}_r(\pi)$) whilst minimizing the constraint functions (i.e., $\mathcal{J}_g^i(\pi)$) if it is violated.

Let τ_c be the tolerance, a newly introduced 'relaxation term' linked to constraints. Theoretically, τ_c decouples the estimated cumulative constraint $\bar{\mathcal{J}}_g^i$ to enhance the transparency of convergence. In practical terms, it serves as a lower boundary indicating the level of constraint limit that can be tolerated. The evaluation of its robustness in Section VI-A ensures that its introduction does not cause additional tuning effort, when introducing constraints.² As shown in

Algorithm 1 (Line 10), and we first judge whether $\bar{\mathcal{J}}_g^i(\pi) \leq \mathbf{b}_i + \tau_c, \forall i \in [1, p]$. If so, the policy update towards minimizing $\mathcal{J}_g^i(\pi)$ is taken, where the approximation of the constraints is: $\bar{\mathcal{J}}_g^i(\pi) = \mathbb{E}[\bar{Z}_t^i(s, a)] = \mathbb{E}[\zeta_{K_{td}}^i(s, a)], \forall i \in [1, p]$; otherwise, we take the policy update towards maximizing $\mathcal{J}_r(\pi)$, where $\bar{\mathcal{J}}_r(\pi) = \mathbb{E}[\bar{Z}_t^0(s, a)] = \mathbb{E}[\zeta_{K_{td}}^0(s, a)]$. Thus, different from the traditional CMDP (i.e., Equation 8), the constrained distributional problem (i.e., CDMDP) is defined as:

$$\max_{\pi} \bar{\mathcal{J}}_r(\pi), \quad \text{s.t.} \quad \bar{\mathcal{J}}_g^i(\pi) \leq \mathbf{b}_i + \tau_c, \quad i = 1, \dots, p \quad (8)$$

B. Control Parameterization

A SADF [19], as shown in Equation 9, is an equivalent and tractable formulation of the original affine feedback prediction control policy proposed in [21]. Importantly, the SADF has fewer decision variables which can decrease computational complexity and improve calculation efficiency.

$$\mathbf{u}_{i|t} = \sum_{k=0}^{i-1} \mathbf{M}_{i-k|t} \mathbf{w}_{k|t} + \mathbf{v}_{i|t} \quad (9)$$

where the \mathbf{M}_t is a lower block diagonal Toeplitz structure. $i \in \mathbb{N}_{[1, N-1]}, j \in \mathbb{N}_{i-1}$ and the open-loop control sequence $\mathbf{v}_{i|t} \in \mathbb{R}, i \in \mathbb{N}_{N-1}$ are decision variables at each time step t .

According to [66], the predicted cost can be transformed as:

$$\begin{aligned} \mathcal{L}(\mathbf{x}_t, \mathbf{u}_t) &= \mathcal{L}_N(\mathbf{x}_t, \mathbf{M}_t, \mathbf{v}_t) \\ &= \|\mathbf{H}_x \mathbf{x} + \mathbf{H}_u \mathbf{v}\|_2^2 + \mathbb{E}[\|(\mathbf{H}_u \mathbf{M} \mathbf{G} + \mathbf{H}_w) \mathbf{w}\|_2^2] \end{aligned} \quad (10)$$

where \mathbf{H}_x and \mathbf{H}_u are coefficient matrices which are constructed from Equation 10. $\mathcal{G} := \mathbf{I}_N \otimes \mathbf{G}$ denotes Kronecker product of matrices \mathbf{I}_N and \mathbf{G} . For the convexity guarantee, the matrix $(\mathbf{H}_u \mathbf{M} \mathbf{G} + \mathbf{H}_w)$ is positive semidefinite (see *Proposition 5* in Section V-B and *Proposition 4.4* in [73]). Thus, the

²In the benchmark [12], additional hyperparameters including learning rates are verified to demonstrate their robustness.

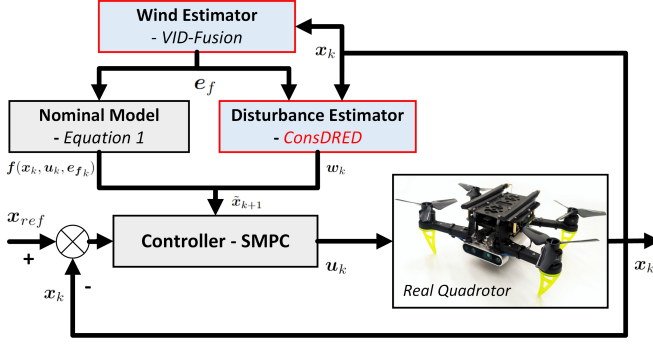


Fig. 1: ConsDRED-SMPC: (i) a wind estimator, i.e., VID-Fusion [16]; (ii) an aerodynamic disturbance estimator, i.e., the proposed ConsDRED (described by Algorithm 1); and (iii) a controller, i.e., SMPC.

optimal control problem, reformulated by SADF (Equation 9), is as follows:

$$\begin{aligned}
 & \min_{\mathbf{M}_t, \mathbf{v}_t} \mathcal{L}_N(\mathbf{x}_t, \mathbf{M}_t, \mathbf{v}_t), \quad \text{s.t. } \forall w_{i|t} \in \mathbb{W}, \forall i \in \mathbb{N}_{N-1} \\
 & \text{subject to } \mathbf{x}_t = \mathbf{A}\mathbf{x}_{0|t} + \mathbf{B}\mathbf{u}_t + \mathbf{G}\mathbf{w}_t \\
 & \quad \mathbf{u}_{i|t} = \sum_{k=0}^{i-1} \mathbf{M}_{i-k|t} \mathbf{w}_{k|t} + \mathbf{v}_{i|t} \\
 & \quad H_u \mathbf{M} \mathbf{G} + H_w \geq 0 \quad (\mathbf{x}_t, \mathbf{u}_t) \in \mathbb{Z} \\
 & \quad \mathbf{x}_{N|t} \in \mathbb{X}_f \quad \mathbf{x}_{0|t} = \mathbf{x}_t
 \end{aligned} \tag{11}$$

The optimal control problem is a strictly convex quadratic program, or second-order cone program (SOCP) if \mathbb{W} is a polytope or ellipsoid when \mathbb{Z} and \mathbb{X}_f are polytopic [66]. In this case, the problem can be seen as deterministic MPC with nonlinear constraints, which can be solved by some nonlinear MPC solvers, e.g., CasADi [67] and ACADOS [74].

C. The Whole Tracking Framework: ConsDRED-SMPC

The objective of this work is to design a quadrotor tracking controller achieving accurate aerodynamic effect estimation, which we define as combined wind estimation and aerodynamic disturbance estimation, for tracking the trajectory reference $\mathbf{x}_{m,t}$ from Kino-JSS [5] accurately. The immediate reward r_{t+1} is defined as:

$$r_{t+1} = -(\mathbf{x}_t - \mathbf{x}_{m,t})^T H_1 (\mathbf{x}_t - \mathbf{x}_{m,t}) - \mathbf{u}_t^T H_2 \mathbf{u}_t \tag{12}$$

where H_1 and H_2 are positive definite matrices. Then we use the DDPG architecture [9] for continuous and high-dimensional disturbance estimation.

The overall control framework for the quadrotor is shown in Fig. 1. The SADF in ConsDRED and SMPC are shown in Algorithm 1 and Algorithm 2, respectively.

V. PROPERTIES OF CONSDRED-SMPC

In this section, the properties of the proposed control framework ConsDRED-SMPC are analyzed, including convergence of ConsDRED and stability guarantees of the Controller SADF-SMPC.

A. Convergence Analysis of ConsDRED

We present *Proposition 2* and *Proposition 3* on the convergence analysis for the Distributional RL (ConsDRED) in Section IV-A.

Lemma 1 ([47]): The Bellman operator \mathcal{T}^π is a p -contraction under the p -Wasserstein metric \bar{d}_p .

Lemma 1 suggests that an effective practical way to minimize the Wasserstein distance between a distribution Z and its Bellman update $\mathcal{T}^\pi Z$ can be found in Equation 4, which attempts iteratively to minimize the L_2 distance between Z and $\mathcal{T}^\pi Z$ in TD learning.

Proposition 2 (Policy Evaluation): Let Π_{W_1} be a quantile approximation under the minimal 1-Wasserstein distance W_1 , \mathcal{T}^π be the Bellman operator under a deterministic policy π and $Z_{k+1}(s, \mathbf{a}) = \Pi_{W_1} \mathcal{T}^\pi Z_k(s, \mathbf{a})$. The sequence $Z_k(s, \mathbf{a})$ converges to a unique fixed point \tilde{Z}_π under the maximal form of ∞ -Wasserstein metric \bar{d}_∞ .

Proof: Equation 5 implies that the combined operator $\Pi_{W_1} \mathcal{T}^\pi$ is an ∞ -contraction [17]. We conclude using Banach's fixed point theorem that \mathcal{T}^π has a unique fixed point, i.e., \tilde{Z}_π . Furthermore, Equation 7 implies that all moments of Z are bounded. Therefore, we conclude that the sequence $Z_k(s, \mathbf{a})$ converges to \tilde{Z}_π in \bar{d}_∞ for $p \in [1, \infty]$. ■

Proposition 3 (Policy Improvement): Let π_{old} be an old policy, π_{new} be a new policy and $Q(s, \mathbf{a}) = \mathbb{E}[Z(s, \mathbf{a})]$ in Equation 7. There exists $Q^{\pi_{new}}(s, \mathbf{a}) \geq Q^{\pi_{old}}(s, \mathbf{a})$, $\forall s \in \mathcal{S}$ and $\forall \mathbf{a} \in \mathcal{A}$.

Proof: Based on Equation 7, there exists:

$$\begin{aligned}
 V^\pi(s_t) &= \mathbb{E}_\pi Q^\pi(s_t, \pi(s_t)) \leq \max_{\mathbf{a} \in \mathcal{A}} \mathbb{E}_\pi Q^\pi(s_t, \mathbf{a}) \\
 &= \mathbb{E}_{\pi'} Q^\pi(s_t, \pi'(s_t))
 \end{aligned} \tag{13}$$

where $\mathbb{E}_\pi[\cdot] = \sum_{\mathbf{a} \in \mathcal{A}} \pi(\mathbf{a}|s)[\cdot]$, and $V^\pi(s) = \mathbb{E}_\pi \mathbb{E}[Z_k(s, \mathbf{a})]$ is the value function. According to Equation 13 and Equation 7, it yields:

$$\begin{aligned}
 Q^{\pi_{old}} &= Q^{\pi_{old}}(s_t, \pi_{old}(s_t)) \\
 &= r_{t+1} + \gamma \mathbb{E}_{s_{t+1}} \mathbb{E}_{\pi_{old}} Q^{\pi_{old}}(s_{t+1}, \pi_{old}(s_{t+1})) \\
 &\leq r_{t+1} + \gamma \mathbb{E}_{s_{t+1}} \mathbb{E}_{\pi_{new}} Q^{\pi_{old}}(s_{t+1}, \pi_{new}(s_{t+1})) \\
 &\leq r_{t+1} + \mathbb{E}_{s_{t+1}} \mathbb{E}_{\pi_{new}} [\gamma r_{t+2} \\
 &\quad + \gamma^2 \mathbb{E}_{s_{t+2}} Q^{\pi_{old}}(s_{t+2}, \pi_{new}(s_{t+2}))] \\
 &\leq r_{t+1} + \mathbb{E}_{s_{t+1}} \mathbb{E}_{\pi_{new}} [\gamma r_{t+2} + \gamma^2 r_{t+3} + \dots] \\
 &= r_{t+1} + \mathbb{E}_{s_{t+1}} V^{\pi_{new}}(s_{t+1}) \\
 &= Q^{\pi_{new}}
 \end{aligned} \tag{14}$$

Given *Proposition 2* and *Proposition 3*, we can now analyze the convergence of the ConsDRED.

Theorem 1 (Global Convergence): Let π^i be the policy in the i -th policy improvement, $i = 1, 2, \dots, \infty$, and $\pi^i \rightarrow \pi^*$ when $i \rightarrow \infty$. There exists $Q^{\pi^*}(s, \mathbf{a}) \geq Q^{\pi^i}(s, \mathbf{a})$, $\forall s \in \mathcal{S}$ and $\forall \mathbf{a} \in \mathcal{A}$.

Proof: Since *Proposition 3* suggests $Q^{\pi^{i+1}}(s, \mathbf{a}) \geq Q^{\pi^i}(s, \mathbf{a})$, the sequence $Q^{\pi^i}(s, \mathbf{a})$ is monotonically increasing where $i \in \mathbb{N}$ is the policy iteration step. Furthermore, *Lemma 1* implies that the state-action distribution Z over \mathbb{R} has bounded

p -th moment, so the first moment of Z , i.e., $Q^{\pi_i}(s, a)$, is upper bounded. Therefore, the sequence $Q^{\pi_i}(s, a)$ converges to an upper limit $Q^{\pi^*}(s, a)$ with $\forall s \in \mathcal{S}$ and $\forall a \in \mathcal{A}$. ■

Next we present the convergence rate both for the *TD learning* (defined in Equation 6) and global *Constrained Distributional Reinforcement Learning* (defined in Equation 8). Let q_i be the quantile distribution supports, which equals to the outputs of the H -layer neural networks $f^{(h)}$: $q_i = f^{(H)}$. The H -layer neural networks are defined as [75]: $x^{(h)} = \frac{1}{\sqrt{m}} \mathbf{1}(\theta^{(h)} x^{(h-1)} > 0) \cdot \theta^{(h)} x^{(h-1)}$, $f^{(H)}(x) = (s, a, \theta_K^Q) = b_r x^H$, $\forall h \in [2, H]$, where the neural network parameters are bounded as $\|\theta\|_2 \leq d_\theta$. The $f_0^{(H)}$ is defined as: $f_0^{(H)} = b_r x_0^{(H)}$, $x_0^{(h)}((s, a, \theta_K^Q) = \frac{1}{\sqrt{m}} \mathbf{1}(\theta^{(0)} x_0^{(h-1)} > 0) \cdot \theta^{(h)} x_0^{(h-1)}$.

Proposition 4 (Convergence rate of neural TD learning):

Let m be the width of the actor-critic networks, and $\bar{Z}_t = \frac{1}{N} \sum_{i=1}^N \delta_{q_i(s, a)}$ be an estimator of Z_t^i . In the TD learning, with probability at least $1 - \delta$, there exists

$$\left\| \Pi_{W_1} \bar{Z}_t - \Pi_{W_1} Z_t^* \right\| \leq \Theta(m^{-\frac{H}{4}}) + \Theta([(1 - \gamma)K]^{-\frac{1}{2}} [1 + \log^{\frac{1}{2}} \delta^{-1}]) \quad (15)$$

Proof: Based on Gluing lemma of Wasserstein distance W_p [76], [77], there exists:

$$\begin{aligned} \left\| \Pi_{W_1} \bar{Z}_t - \Pi_{W_1} Z_t^* \right\| &= \sum_{i=1}^N \left\| \bar{q}_t^i - q_t^{i,*} \right\| \\ &= \sum_{i=1}^N \left\| f_i^{(H)}((s, a), \theta_{K_{td}}^Q) - f_i^{(H)}((s, a), \theta^{Q^*}) \right\| \\ &\leq \sum_{i=1}^N \left\| f_i^{(H)}((s, a), \theta_{K_{td}}^Q) - f_{0,i}^{(H)}((s, a), \theta^Q) \right\| \\ &+ \sum_{i=1}^N \left\| f_{0,i}^{(H)}((s, a), \theta_{K_{td}}^Q) - f_i^{(H)}((s, a), \theta^{Q^*}) \right\| \\ &\stackrel{(i)}{\leq} \Theta(m^{-\frac{H}{4}}) + \sum_{i=1}^N \left\| f_{0,i}^{(H)}((s, a), \theta_{K_{td}}^Q) - f_i^{(H)}((s, a), \theta^{Q^*}) \right\| \\ &\stackrel{(ii)}{\leq} \Theta(m^{-\frac{H}{4}}) + \Theta([(1 - \gamma)K_{td}]^{-\frac{1}{2}} [1 + \log^{\frac{1}{2}} \delta^{-1}]) \end{aligned} \quad (16)$$

where (i) follows from [75] (Lemma 5.1):

$$\begin{aligned} \sum_{i=1}^N \left\| f_i^{(H)}((s, a), \theta_{K_{td}}^Q) - f_{0,i}^{(H)}((s, a), \theta^Q) \right\|^2 &\leq \frac{1}{m^H} \sum_{i=1}^N b_r \\ &\left| [(1(W_i^{(h)} x_i^{(h-1)} > 0) - 1(W_i^{(0)} x_i^{(h-1)} > 0)) \cdot W_i^{(h)} x_i^{(h-1)}]^2 \right| \\ &\leq \frac{4C_0}{m^H} \sum_{i=1}^N \sum_{r=1}^m \mathbf{1}(|W_{i,r}^{(0)} x_i^{(h-1)}| \leq \|W_{i,r}^{(h)} - W_{i,r}^{(0)}\|_2) \\ &\leq \frac{4C_0}{m^H} \left(\sum_{i=1}^N \sum_{r=1}^m \|W_{i,r}^{(h)} - W_{i,r}^{(0)}\|_2^2 \right)^{\frac{1}{2}} \left(\sum_{r=1}^m \left\| \frac{1}{W_{i,r}^{(0)}} \right\|_2^2 \right)^{\frac{1}{2}} \leq \frac{4C_0 C_1}{m^{\frac{H}{2}}} \end{aligned} \quad (17)$$

Algorithm 1 ConsDRED

Input: $s_k, s_{k+1}, u_k, \theta^\mu, \theta^Q$

Output: a_k

1: **Initialize:**

- $\theta = [\theta^\mu, \theta^Q]$: the parameters of actor network θ^μ , and the parameters of critic network θ^Q
- the replay memory $D \leftarrow D_{k-1}$
- the batch B , and its size
- the random option selection probability ϵ
- the option termination probability β

2: **Repeat**

3: **for** $t = 0, 1, 2, \dots, T - 1$ **do**

- 4: Select action $a_t = \pi(s_t | \theta^\mu + \mathcal{N}_t)$ based on the current policy and exploration Gaussian noise
- 5: Execute action a_t (i.e., w_k in Algorithm 2), get reward r_t and the next state s_{t+1}
- 6: $D.\text{insert}([s_k, a_k, r_k, s_{k+1}])$, and $([s_n, a_n, r_n, s_{n+1}])$ of N tuples $\in B \leftarrow D.\text{sampling}$
- 7: **policy evaluation:** $z_{t,n}^i \leftarrow \zeta_{K_{td}}^i(s, a)$, $\forall i \in [0, p]$
- 8: **constraint estimation:** compute the constraint estimation: $\bar{\mathcal{J}}_g^i(\pi(s, a)) = \mathbb{E}[\zeta_{K_{td}}^i(s, a)]$, $\forall i \in [1, p]$

9: **policy improvement:**

10: **if** $\bar{\mathcal{J}}_g^i(\pi) \leq b_i + \tau_c$ **then**

- 11: Update the policy towards maximizing $\mathcal{J}_r(\pi)$:
compute the actor update: $\delta_{\theta^\mu} \leftarrow (1/N) \sum_{n=0} \nabla_{\theta^\mu} \pi_{\theta^\mu}(s_n) \mathbb{E}[\nabla_a Z_{\theta^Q}(s_n, a)]_{a=\pi_{\theta^\mu}(s_n)}$
compute the critic update: $\delta_{\theta^Q} \leftarrow (1/N) \sum_{n=0} \nabla_{\theta^Q} \bar{d}_\infty(\Pi_{W_1} \mathcal{T}^\pi Z_{\theta^Q}(s_n, a_n), \Pi_{W_1} \mathcal{T}^\pi z_{t,n}^0)$
 $\theta^\mu \leftarrow \theta^\mu + l_\mu \delta_{\theta^\mu}$, and $\theta^Q \leftarrow \theta^Q + l_\theta \delta_{\theta^Q}$

12: **else**

- 13: Update the policy towards minimizing $\mathcal{J}_g^i(\pi)$:
 $\theta^\mu \leftarrow \theta^\mu - l_\mu \nabla_{\theta^\mu} \zeta_{K_{td}}^i$, and $\theta^Q \leftarrow \theta^Q - l_\theta \nabla_{\theta^Q} \zeta_{K_{td}}^i$,
 $\forall i \in [1, p]$

14: **end if**

15: **end for**

where the constant $C_0 > 0$ and $C_1 > 0$. Thus we upper bound $\sum_{i=1}^N \|f_i^{(H)} - f_{0,i}^{(H)}\| \leq \Theta(m^{-\frac{H}{4}})$, which holds (i) in Equation 16. Then (ii) follows from [78] (Lemma 1), with probability at least $1 - \delta$, there exists:

$$\begin{aligned} \sum_{i=1}^N \left\| f_{0,i}^{(H)}((s, a), \theta_{K_{td}}^Q) - f_i^{(H)}((s, a), \theta^{Q^*}) \right\| &\leq \frac{1}{\sqrt{1 - \gamma}} \sum_{i=1}^N \left\| f_{0,i}^{(H)}((s, a), \theta_{K_{td}}^Q) - f_i^{(H)}((s, a), \theta^{Q^*}) \right\| \\ &\leq \frac{C_3}{\sqrt{(1 - \gamma)K_{td}}} (1 + \sqrt{\log \frac{1}{\delta}}) \end{aligned} \quad (18)$$

where (ii) holds, and therefore Equation 16 holds. ■

Proposition 4 suggests that given the deterministic hyperparameters, i.e., H -layer networks with width m and the CDMDP discount rate γ , and after executing the TD-learning

iterations in Equation 6 for $\Theta(m^{\frac{H}{2}})$, the approximation \bar{Z}_t can be achieved by $\left\| \Pi_{W_1} \bar{Z}_t - \Pi_{W_1} Z_t^* \right\| \leq \Theta(m^{-\frac{H}{4}})$ with high probability.

Theorem 2 (Global Convergence Rate): In the training process of CDMDP (i.e., Algorithm 1): employ the neural TD in Equation 6 with $K_{td} = (1-\gamma)^{-\frac{3}{2}} m^{\frac{H}{2}}$, let the policy update (in Line 13 of Algorithm 1) be $l_Q = \frac{1}{\sqrt{T}}$ and the tolerance be $\tau_c = \Theta(\frac{1}{(1-\gamma)\sqrt{T}}) + \Theta(\frac{1}{(1-\gamma)Tm^{\frac{H}{4}}})$, with probability at least $1 - \delta$, there exists

$$\begin{aligned} \mathcal{J}_r(\pi^*) - \mathbb{E}[\bar{\mathcal{J}}_r(\pi)] &\leq \Theta\left(\frac{1}{(1-\gamma)\sqrt{T}}\right) \\ &+ \Theta\left(\frac{1}{(1-\gamma)Tm^{\frac{H}{4}}} \sqrt{\log \frac{1}{\delta}}\right) \end{aligned} \quad (19)$$

Then for the constraint approximation $\bar{\mathcal{J}}_g^i(\pi)$, $\forall i \in [1, p]$, there exists

$$\begin{aligned} \mathbb{E}[\bar{\mathcal{J}}_g^i(\pi)] - b_i &\leq \Theta\left(\frac{1}{(1-\gamma)\sqrt{T}}\right) \\ &+ \Theta\left(\frac{1}{(1-\gamma)Tm^{\frac{H}{4}}} \sqrt{\log \frac{1}{\delta}}\right) \end{aligned} \quad (20)$$

Proof: Let $\Delta_{\theta Q} = \theta_{t+1}^Q - \theta_t^Q$. Suppose the critic networks are H -layer neural networks. Based on [79] (Lemma 6.1), there exists

$$\begin{aligned} (1-\gamma)[\mathcal{J}_r(\pi^*) - \bar{\mathcal{J}}_r(\pi_t)] &= \mathbb{E}[Q_{\pi_t}(s, a) - \mathbb{E}Q_{\pi_t}(s, a')] \\ &= \mathbb{E}[\nabla_{\theta} f^{(H)}((s, a), \theta^Q)^T - \mathbb{E}[\nabla_{\theta} f^{(H)}((s, a'), \theta^Q)^T]] \Delta_{\theta Q} \\ &+ \mathbb{E}[Q_{\pi_t}(s, a) - \nabla_{\theta} f^{(H)}((s, a), \theta^Q)^T \Delta_{\theta Q}] \\ &+ \mathbb{E}[\nabla_{\theta} f^{(H)}((s, a'), \theta^Q)^T \Delta_{\theta Q} - Q_{\pi_t}(s, a')] \\ &= \frac{1}{l_Q} [l_Q \mathbb{E}[\nabla_{\theta} \log(\pi_t(a|s))^T] \Delta_{\theta Q} - \frac{l_Q^2 \mathcal{L}_f}{2} \|\Delta_{\theta Q}\|_2^2] \\ &+ \mathbb{E}[Q_{\pi_t}(s, a) - \nabla_{\theta} f^{(H)}((s, a), \theta^Q)^T \Delta_{\theta Q}] \\ &+ \frac{l_Q \mathcal{L}_f}{2} \|\Delta_{\theta Q}\|_2^2 \\ &+ \mathbb{E}[\nabla_{\theta} f^{(H)}((s, a'), \theta^Q)^T \Delta_{\theta Q} - Q_{\pi_t}(s, a')] \\ &\stackrel{(i)}{\leq} \frac{1}{l_Q} \mathbb{E}[\log(\frac{\pi_{t+1}(a|s)}{\pi_t(a|s)})] + \frac{l_Q \mathcal{L}_f}{2} \|\Delta_{\theta Q}\|_2^2 \\ &+ \sqrt{\mathbb{E}[Q_{\pi_t}(s, a) - f^{(H)}((s, a), \Delta_{\theta Q})]^2} \\ &+ \sqrt{\mathbb{E}[f^{(H)}((s, a), \Delta_{\theta Q}) - \nabla_{\theta} f^{(H)}((s, a), \theta^Q)^T \Delta_{\theta Q}]^2} \\ &+ \sqrt{\mathbb{E}[\nabla_{\theta} f^{(H)}((s, a'), \theta^Q)^T \Delta_{\theta Q} - f^{(H)}((s, a'), \Delta_{\theta Q})]^2} \\ &+ \sqrt{\mathbb{E}[f^{(H)}((s, a'), \Delta_{\theta Q}) - Q_{\pi_t}(s, a')]^2} \\ &= \frac{1}{l_Q} [\mathbb{E}[\mathcal{D}_{KL}(\pi^* || \pi_t)] - \mathbb{E}[\mathcal{D}_{KL}(\pi^* || \pi_{t+1})]] \\ &+ 2\sqrt{\mathbb{E}[f^{(H)}((s, a), \Delta_{\theta Q}) - \nabla_{\theta} f^{(H)}((s, a), \theta^Q)^T \Delta_{\theta Q}]^2} \\ &+ 2\sqrt{\mathbb{E}[Q_{\pi_t}(s, a) - f^{(H)}((s, a), \Delta_{\theta Q})]^2} + \frac{l_Q \mathcal{L}_f}{2} \|\Delta_{\theta Q}\|_2^2 \end{aligned} \quad (21)$$

where (i) follows from the \mathcal{L}_f -Lipschitz property of $\log(\pi_t(a|s))$. Next, we upper bound the term $\sqrt{\mathbb{E}[f^{(H)}((s, a), \Delta_{\theta Q}) - \nabla_{\theta} f^{(H)}((s, a), \theta^Q)^T \Delta_{\theta Q}]^2}$ as shown below.

$$\begin{aligned} &\sqrt{\mathbb{E}[f^{(H)}((s, a), \Delta_{\theta Q}) - \nabla_{\theta} f^{(H)}((s, a), \theta^Q)^T \Delta_{\theta Q}]^2} \\ &= \sum_{i=1}^N \left\| f_i^{(H)}((s, a), \Delta_{\theta Q}) - \nabla_{\theta} f_i^{(H)}((s, a), \theta^Q)^T \Delta_{\theta Q} \right\| \\ &\leq \sum_{i=1}^N \left[\left\| f_i^{(H)}((s, a), \Delta_{\theta Q}) - \nabla_{\theta} f_{0,i}^{(H)}((s, a), \theta^Q)^T \Delta_{\theta Q} \right\| \right. \\ &\quad \left. + \left\| \nabla_{\theta} f_{0,i}^{(H)}((s, a), \theta^Q)^T \Delta_{\theta Q} - \nabla_{\theta} f_i^{(H)}((s, a), \theta^Q)^T \Delta_{\theta Q} \right\| \right] \\ &= 2 \sum_{i=1}^N \left\| f_i^{(H)}((s, a), \Delta_{\theta Q}) - f_{0,i}^{(H)}((s, a), \Delta_{\theta Q}) \right\| \\ &\stackrel{(ii)}{\leq} \frac{4\sqrt{C_0 C_1}}{m^{\frac{H}{4}}} \end{aligned} \quad (22)$$

where (ii) follows from Equation 17. Then, in order to upper bound $\sqrt{\mathbb{E}[Q_{\pi_t}(s, a) - f^{(H)}((s, a), \Delta_{\theta Q})]^2}$, taking expectation of Equation 21 from $t = 0$ to $T - 1$, yields

$$\begin{aligned} (1-\gamma)[\mathcal{J}_r(\pi^*) - \mathbb{E}[\bar{\mathcal{J}}_r(\pi)]] &= (1-\gamma) \frac{1}{T} \sum_{t=0}^{T-1} [\mathcal{J}_r(\pi^*) - \bar{\mathcal{J}}_r(\pi_t)] \\ &\leq \frac{1}{T} \left[\frac{1}{l_Q} \mathbb{E}[\mathcal{D}_{KL}(\pi^* || \pi_t)] + \frac{8T\sqrt{C_0 C_1}}{m^{\frac{H}{4}}} + \frac{Tl_Q \mathcal{L}_f}{2} d_{\theta}^2 \right. \\ &\quad \left. + 2 \sum_{t=0}^{T-1} \sum_{i=1}^N \left\| f_i^{(H)}((s, a), \theta_{t+1}^Q - \theta_t^Q) - f_i^{(H)}((s, a), \theta^{Q^*}) \right\| \right] \\ &= \frac{\mathbb{E}[\mathcal{D}_{KL}(\pi^* || \pi_t)]}{l_Q T} + \frac{8\sqrt{C_0 C_1}}{m^{\frac{H}{4}}} + \frac{l_Q \mathcal{L}_f}{2} d_{\theta}^2 \\ &\quad + \frac{2}{T} \sum_{i=1}^N \left\| f_i^{(H)}((s, a), \theta_{K_{td}, t}^Q) - f_i^{(H)}((s, a), \theta^{Q^*}) \right\| \\ &\stackrel{(iii)}{\leq} \frac{\mathbb{E}[\mathcal{D}_{KL}(\pi^* || \pi_t)]}{l_Q T} + \frac{8\sqrt{C_0 C_1}}{m^{\frac{H}{4}}} + \frac{l_Q \mathcal{L}_f}{2} d_{\theta}^2 \\ &\quad + \frac{4\sqrt{C_0 C_1}}{Tm^{\frac{H}{4}}} + \frac{2C_3}{T\sqrt{(1-\gamma)K_{td}}} (1 + \sqrt{\log \frac{1}{\delta}}) \end{aligned} \quad (23)$$

where (iii) follows from Proposition 4 (Equation 16). Thus, substituting $K_{td} = (1-\gamma)^{-1} m^{\frac{H}{2}}$ and $l_Q = \Theta(1/\sqrt{T})$ into Equation 23, with probability at least $1 - \delta$, yields:

$$\begin{aligned} \mathcal{J}_r(\pi^*) - \mathbb{E}[\bar{\mathcal{J}}_r(\pi)] &\leq C_5 \frac{1}{(1-\gamma)\sqrt{T}} + C_6 \frac{1}{(1-\gamma)m^{\frac{H}{4}}} \\ &\quad + C_7 \frac{1}{(1-\gamma)Tm^{\frac{H}{4}}} + 2C_3 \frac{\sqrt{\log \frac{1}{\delta}}}{(1-\gamma)Tm^{\frac{H}{4}}} \\ &\leq \Theta\left(\frac{1}{(1-\gamma)\sqrt{T}}\right) + \Theta\left(\frac{1}{(1-\gamma)Tm^{\frac{H}{4}}} \sqrt{\log \frac{1}{\delta}}\right) \end{aligned} \quad (24)$$

where $C_5 = \mathbb{E}[\mathcal{D}_{KL}(\pi^* || \pi_t)] + \frac{\mathcal{L}_f d_{\theta}^2}{2}$, $C_6 = 8\sqrt{C_0 C_1}$ and $C_7 = 4\sqrt{C_0 C_1} + 2C_3$. Therefore, Equation 19 holds.

Algorithm 2 SADP-SMPC

```

1: Get:
   - the reference data  $\mathbf{x}_{ref}$  from the quadrotor trajectory
     planning and generation module, i.e., Kino-JSS [5]
   - the measurement state  $\mathbf{x}_k$  from on-board depth camera
     and IMU (see Table III for details please)
   - the wind estimation  $\mathbf{e}_{fk}$  from VID-Fusion [16]
2: Initialize:
   - the parameters  $\theta^\mu$  and  $\theta^Q$  for the actor  $\mu$  and the critic
      $Q$ , respectively
   - the decision variables  $\mathbf{M}_0$  and  $\mathbf{v}_0$  in Equation 9
   - the initial state  $\mathbf{s}_0$ 
3: for each sampling timestamps  $k$  do
4:   Repeat
5:      $\mathbf{s}_k \leftarrow [\mathbf{x}_k, \mathbf{e}_{fk}]$ 
6:     Select an action vector  $\mathbf{w}_k \leftarrow [w_{0|k}^T, w_{1|k}^T, \dots, w_{N|k}^T]^T$ 
       from  $\mathbf{w}_k = \mathbf{a}_k \leftarrow \mu(\mathbf{a}_k | \mathbf{s}_k)$  in ConsDRED (Algo-
       rithm 1)
7:      $\mathbf{u}_{i|k} \leftarrow \sum_{l=0}^{i-1} \mathbf{M}_{i-l|k} \mathbf{w}_{l|k} + \mathbf{v}_{i|k}$ 
8:      $\mathbf{u}_k \leftarrow \mathbf{u}_{0|k}, \mathbf{w}_k \leftarrow \mathbf{w}_{0|k}$ 
9:      $\mathbf{x}_k \leftarrow \mathbf{A}\mathbf{x}_{0|k} + \mathbf{B}\mathbf{u}_k + \mathbf{G}\mathbf{w}_k$ 
10:    Solve optimization problem Equation 11 with nonlinear
       MPC solver, i.e., ACADOS [74]
11:    Until convergence
12:     $\mathbf{u}_k \leftarrow \mathbf{v}_{0|k}$ 
13:     $\mathbf{x}_{k+1}, \mathbf{e}_{fk+1} \leftarrow \text{RealQuadrotor}(\mathbf{u}_k)$ 
14:     $\mathbf{s}_{k+1} \leftarrow [\mathbf{x}_{k+1}, \mathbf{e}_{fk+1}]$ 
15:     $\mathbf{x}_{ref} \leftarrow \text{Kino-JSS}$ 
16:     $k \leftarrow k + 1$ 
17: end for

```

Following *Line 13* in Algorithm 1 and recalling Equation 21, Equation 22 and Equation 23, the convergence process is similarly stated for the constraint approximation $\bar{\mathcal{J}}_g^i(\pi)$, $\forall i \in [1, p]$ here

$$\begin{aligned} \mathbb{E}[\bar{\mathcal{J}}_g^i(\pi)] - \mathcal{J}_g^i(\pi^*) &\leq \Theta\left(\frac{1}{(1-\gamma)\sqrt{T}}\right) \\ &\quad + \Theta\left(\frac{1}{(1-\gamma)Tm^{\frac{H}{4}}}\sqrt{\log \frac{1}{\delta}}\right) \end{aligned} \quad (25)$$

the constraint violation is then bounded below

$$\begin{aligned} \mathbb{E}[\bar{\mathcal{J}}_g^i(\pi)] - \mathbf{b}_i &\leq [\mathcal{J}_g^i(\pi^*) - \mathbf{b}_i] + [\mathbb{E}[\bar{\mathcal{J}}_g^i(\pi)] - \mathcal{J}_g^i(\pi^*)] \\ &\leq \tau_c + [\mathbb{E}[\bar{\mathcal{J}}_g^i(\pi)] - \mathcal{J}_g^i(\pi^*)] \\ &\leq \tau_c + \Theta\left(\frac{1}{(1-\gamma)\sqrt{T}}\right) + \Theta\left(\frac{1}{(1-\gamma)Tm^{\frac{H}{4}}}\sqrt{\log \frac{1}{\delta}}\right) \end{aligned} \quad (26)$$

where we have $\tau_c = \Theta\left(\frac{1}{(1-\gamma)\sqrt{T}}\right) + \Theta\left(\frac{1}{(1-\gamma)Tm^{\frac{H}{4}}}\right)$, there-

fore, Equation 20 holds: $\mathbb{E}[\bar{\mathcal{J}}_g^i(\pi)] - \mathbf{b}_i \leq \Theta\left(\frac{1}{(1-\gamma)\sqrt{T}}\right) + \Theta\left(\frac{1}{(1-\gamma)Tm^{\frac{H}{4}}}\sqrt{\log \frac{1}{\delta}}\right)$. ■

According to *Theorem 2*, **1)** CDMDP (i.e., Algorithm 1) guarantees convergence to the global optimal policy π^* at a

sublinear rate $\Theta(1/\sqrt{T})$ whilst achieving an approximation error $\Theta(1/m^{\frac{H}{4}})$ decrease as the width and the layer of neural network m and H increase; and **2)** the constraint violation (shown in Equation 20) also converges to zero at a sublinear rate $\Theta(1/\sqrt{T})$ with an error $\Theta(1/m^{\frac{H}{4}})$ decrease as m and H increase. Therefore, to obtain an output policy π_{out} reaching $\mathcal{J}_r(\pi^*) - \mathbb{E}[\mathcal{J}_r(\pi_{out})] \leq \xi$ and $\mathbb{E}[\bar{\mathcal{J}}_g^i(\pi_{out})] - \mathbf{b}_i \leq \xi$, CDMDP needs at most $T = \Theta(\xi^{-2})$ iterations.

B. Stability Guarantee of the Controller

In this subsection, the closed-loop stability of ConsDRED-SMPC control framework will be demonstrated. The closed-loop stability is analyzed under the Lipschitz Lyapunov function [22] to guarantee ISS. Before the closed-loop stability analysis, the convexity and Lipschitz continuity of the cost function $\mathcal{L}_N(\mathbf{x}_t, \mathbf{M}_t, \mathbf{v}_t)$ are introduced in *Proposition 5* and *Proposition 6*, respectively. Since the output of ConsDRED is non-zero-mean and bounded values, which are different from the assumption of zero-mean disturbances in most previous work ([19] and [66]), the following proofs are all based on the non-zero-mean and bounded disturbances.

We first define an optimal control policy based on the affine disturbance feedback control law:

$$(\mathbf{M}^*(x), \mathbf{v}^*(x)) := \arg \min_{(\mathbf{M}, \mathbf{v}) \in \mathcal{V}_N} \mathcal{L}_N(\mathbf{x}, \mathbf{M}, \mathbf{v}) \quad (27)$$

where \mathcal{V}_N is the set of feasible policies, and $(\mathbf{M}^*(x), \mathbf{v}^*(x))$ is a optimal control policy group. The optimal value function $\mathcal{L}_N^*(x)$ under the affine disturbance feedback control law is defined as:

$$\mathcal{L}_N^*(x) := \min_{(\mathbf{M}, \mathbf{v}) \in \mathcal{V}_N} \mathcal{L}_N(\mathbf{x}, \mathbf{M}, \mathbf{v}) \quad (28)$$

Then we demonstrate that the optimal value function $\mathcal{L}_N(x)$ is convex (see *Proposition 5*) so that Equation 28 can be operated as a convex optimization problem.

Proposition 5: The function $\mathcal{L}_N(\mathbf{x}, \mathbf{M}, \mathbf{v})$ is convex.

Proof: In Equation 10, the second term $\mathbb{E}[\|(H_u \mathbf{M} \mathbf{G} + H_w) \mathbf{w}\|_2^2]$, i.e., the expected value of a quadratic form with respect to the vector-valued random variable \mathbf{w} , is equal to:

$$\begin{aligned} \mathbb{E}[\|(H_u \mathbf{M} \mathbf{G} + H_w) \mathbf{w}\|_2^2] &= \mathbb{E}[\text{tr}((H_u \mathbf{M} \mathbf{G} + H_w) \mathbf{w} \mathbf{w}^T)] \\ &= \text{tr}((H_u \mathbf{M} \mathbf{G} + H_w) \mathbb{E}[\mathbf{w} \mathbf{w}^T]) \\ &= \text{tr}((H_u \mathbf{M} \mathbf{G} + H_w) (\text{Cov}(\mathbf{w}) + \boldsymbol{\mu} \boldsymbol{\mu}^T)) \\ &= \text{tr}(\mathbf{C}_w^{\frac{1}{2}} (H_u \mathbf{M} \mathbf{G} + H_w)^T (H_u \mathbf{M} \mathbf{G} + H_w) \mathbf{C}_w^{\frac{1}{2}}) \\ &\quad + \boldsymbol{\mu}^T (H_u \mathbf{M} \mathbf{G} + H_w) \boldsymbol{\mu} \end{aligned} \quad (29)$$

where $\text{tr}(\cdot)$ denotes the trace of a square matrix. $\boldsymbol{\mu} = \mathbb{E}(\mathbf{w})$ is the expected value of \mathbf{w} , and $\mathbf{C}_w = \text{Var}(\mathbf{w})$ is the variance-covariance matrix of \mathbf{w} . Therefore, $\mathcal{L}_N(x)$ can be written as:

$$\begin{aligned} \mathcal{L}_N(x) &= \|\mathbf{H}_x \mathbf{x} + \mathbf{H}_u \mathbf{v}\|_2^2 + \|\boldsymbol{\mu}\|_{(H_u \mathbf{M} \mathbf{G} + H_w)}^2 \\ &\quad + \text{tr}(\mathbf{C}_w^{\frac{1}{2}} (H_u \mathbf{M} \mathbf{G} + H_w)^T (H_u \mathbf{M} \mathbf{G} + H_w) \mathbf{C}_w^{\frac{1}{2}}) \end{aligned} \quad (30)$$

where $\|x\|_P$ denotes weighted 2-norm of the vector x . Equation 30 is convex since it consists of convex functions of vector and matrix norms. ■

Proposition 6: The function $\mathcal{L}_N^*(x, \mathbf{M}, \mathbf{v})$ is Lipschitz continuous.

Proof: The cost function $\mathcal{L}_N(x, \mathbf{M}, \mathbf{v})$ is proved to be convex in *Proposition 5* so that $\mathcal{L}_N^*(x, \mathbf{M}, \mathbf{v})$ is convex if \mathcal{V}_N has a non-empty interior (*Proposition 1* of [66]). Z is a compact (closed and bounded) set so that $\mathcal{L}_N^*(x, \mathbf{M}, \mathbf{v})$, defined under the compact space Z , is piecewise quadratic (*Corollary 4.6* of [73]). Therefore $\mathcal{L}_N^*(x, \mathbf{M}, \mathbf{v})$ is a Lipschitz continuity function. ■

The above results lead directly to our final result:

Theorem 3: Let \mathcal{W} , \mathcal{Z} and \mathcal{X}_f be polytopes. The closed-loop system (Equation 2) under the SADF control law $\mathbf{u}_{i|t}$ (in Equation 9) is ISS. The ISS is also guaranteed in such cases: the stochastic disturbance \mathbf{w}_t is an i.i.d. bounded and non-zero-mean distribution, i.e., $\mathbb{E}(w_k) \neq 0$.

Proof: According to *Proposition 5* and *Proposition 6*, we first state that the optimal value function $\mathcal{L}_N^*(x)$ is a Lipschitz continuity function. The key is then to prove that there exists a Lipschitz continuous function, i.e., $\mathcal{L}_N^*(x)$, to satisfy the Lipschitz-ISS criterion (*Proposition 4.15* in [66]).

According to *Proposition 1*, there exists a baseline control law \mathbf{u}_b ensuring ISS under zero-mean distribution disturbance. Let $V_b(x) = V_{Nb}^*(x) - V_{Nb}^*(0)$ be the Lipschitz continuous Lyapunov function [66], where $V_{Nb}^*(x)$ is the optimal value function under the baseline control law \mathbf{u}_b . Here let $x^+ = f(x, w)$ [66], [65], so there exists:

$$\alpha_1(\|x\|) \leq V_b(x) \leq \alpha_2(\|x\|) \quad (31a)$$

$$V_b(f(x, 0)) - V_b(x) \leq -\alpha_3(\|x\|) \quad (31b)$$

Let $V(x) = \mathcal{L}_N^*(x) - \mathcal{L}_N^*(0)$, where $\mathcal{L}_N^*(x)$ is an optimal value function under the affine disturbance feedback control law with bounded and non-zero-mean disturbance distribution (Equation 28). According to Equation 30, $\mathcal{L}_N^*(x)$ is shown as:

$$\begin{aligned} \mathcal{L}_N^*(x) &= \min \{ \mathcal{L}_N(x) \} \\ &= \min \{ \|H_x x + H_u \mathbf{v}\|_2^2 + \|\boldsymbol{\mu}\|_{(H_u \mathbf{M} \mathbf{G} + H_w)}^2 \\ &\quad + \text{tr}(\mathbf{C}_w^{\frac{1}{2}}(H_u \mathbf{M} \mathbf{G} + H_w)^T (H_u \mathbf{M} \mathbf{G} + H_w) \mathbf{C}_w^{\frac{1}{2}}) \} \\ &= V_{Nb}^*(x) + \min \{ \|\boldsymbol{\mu}\|_{(H_u \mathbf{M} \mathbf{G} + H_w)}^2 \} \end{aligned} \quad (32)$$

where $\boldsymbol{\mu}$ is the expected value of disturbances, which is independent with \mathbf{v} and \mathbf{M} . $V(x) = \mathcal{L}_N^*(x) - \mathcal{L}_N^*(0) = V_{Nb}^*(x) - V_{Nb}^*(0) = V_b(x)$. Hence, there exists \mathcal{H}_∞ -functions $\alpha_1(\cdot)$, $\alpha_2(\cdot)$ such that Equation 31a holds with $V_b(\cdot) = V(\cdot) = \mathcal{L}_N^*(\cdot) - \mathcal{L}_N^*(0)$.

To prove $V(\cdot)$ satisfying Equation 31b, note that $V_b(f(x, 0)) - V_b(x) = [V_{Nb}^*(f(x, 0)) - V_{Nb}^*(0)] - [V_{Nb}^*(x) - V_{Nb}^*(0)] = V_{Nb}^*(f(x, 0)) - V_{Nb}^*(x)$, so that $V_{Nb}^*(f(x, 0)) - V_{Nb}^*(x) \leq -\alpha_3(\|x\|)$. It follows that:

$$\begin{aligned} V(f(x, 0)) - V(x) &= [\mathcal{L}_N^*(f(x, 0)) - \mathcal{L}_N^*(0)] - [\mathcal{L}_N^*(x) - \mathcal{L}_N^*(0)] \\ &= \mathcal{L}_N^*(f(x, 0)) - \mathcal{L}_N^*(x) \end{aligned} \quad (33)$$

where both $\mathcal{L}_N^*(f(x, 0))$ and $V_{Nb}^*(f(x, 0))$ have $w = 0$. The only difference between the two control laws is zero-mean or non-zero-mean disturbance distributions so that

TABLE II: Parameters of ConsDRED-SMPC

Parameters	Definition	Values
l_μ	Learning rate of actor	0.001
l_θ	Learning rate of critic	0.001
μ	Actor neural network: fully connected with H hidden layers (m neurons per hidden layer)	-
θ	Critic neural network: fully connected with H hidden layers (m neurons per hidden layer)	-
D	Replay memory capacity	10^6
B	Batch size	128
γ	Discount rate	0.998
-	Training episodes	1000
m	the width of neural network	32
H	the layer of neural network	2
T	Length in each episode	200
T_s	MPC Sampling period	50ms
N	Time steps	20

$\mathcal{L}_N^*(f(x, 0)) = V_{Nb}^*(f(x, 0))$. Hence, combining with Equation 32, Equation 33 can be rewritten as:

$$\begin{aligned} V(f(x, 0)) - V(x) &= V_{Nb}^*(f(x, 0)) - V_{Nb}^*(x) - \min \{ \|\boldsymbol{\mu}\|_{(H_u \mathbf{M} \mathbf{G} + H_w)}^2 \} \end{aligned} \quad (34)$$

According to *Proposition 5*, we have $\min \{ \|\boldsymbol{\mu}\|_{(H_u \mathbf{M} \mathbf{G} + H_w)}^2 \} \geq 0$. Then we have:

$$\begin{aligned} V(f(x, 0)) - V(x) &\leq V_{Nb}^*(f(x, 0)) - V_{Nb}^*(x) \leq -\alpha_3(\|x\|) \end{aligned} \quad (35)$$

Equation 35 above shows that there exists \mathcal{H}_∞ -functions $\alpha_3(\cdot)$ such that Equation 31b holds with $V(\cdot) = \mathcal{L}_N^*(\cdot) - \mathcal{L}_N^*(0)$. Therefore, $V(x) = \mathcal{L}_N^*(x) - \mathcal{L}_N^*(0)$ is a Lipschitz continuous Lyapunov function, and the ISS of the closed-loop system (Equation 2) is guaranteed with bounded and non-zero-mean distribution disturbances, i.e., $\mathbb{E}(w_k) \neq 0$. ■

VI. NUMERICAL EXAMPLE

This section shows the whole training process in both RotorS [80], a UAV gazebo simulator³, and real-world scenarios, where empirical convergence results are consistent with our understanding from theoretical analysis in Section V-A. Then the comparative performance of our proposed ConsDRED-SMPC is evaluated in both simulated and real-world flight experiments, respectively.

A. Comparative performance of ConsDRED Training

Training in challenging environments, particularly directly in real physical environments, is regularly performed by robotics researchers given that such real-world training is known to avoid overfitting and improves generalization, as necessary for shallow neural networks (e.g., the 2-hidden-layer networks used in our proposed ConsDRED). The whole training process is implemented firstly in the simulator before being redeployed in the challenging real-world environments. We transition to the online physical training only when the corresponding constraint value converges below the constraint

³We simulate external winds in gazebo by incorporating a plugin file. The rationale behind this simulation is to emulate the forces acting on exerted on a body, assuming them as external aerodynamic effects.

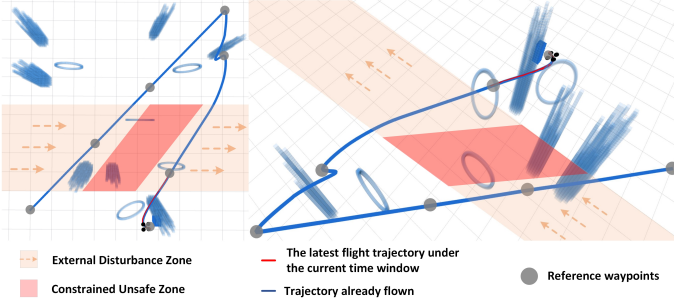


Fig. 2: The simulation scenario: both reference trajectories with/without external forces are generated by Kino-JSS [5].

limit or demonstrates stable convergence if consistently above the limit, as depicted in Fig. 3 (b).

Training Setting: the quadrotor state \mathbf{x} is recorded at 16 Hz. The whole training process occurs over 1000 iterations, within which the simulated training is terminated and transferred to the real-world training, described in Fig. 5, Fig. 6 and Fig. 7.

The matrices H_1 and H_2 in Equation 12 are chosen as $H_1 = \text{diag}\{2.5e^{-2}, 2.5e^{-2}, 2.5e^{-2}, 1e^{-3}, 1e^{-3}, 1e^{-3}, 2.5e^{-3}, 2.5e^{-3}, 2.5e^{-3}, 1e^{-5}, 1e^{-5}, 1e^{-5}\}$ and $H_2 = \text{diag}\{1.25e^{-4}, 1.25e^{-4}, 1.25e^{-4}, 1.25e^{-4}\}$, respectively. Based on the benchmark [5], [18], [12], the parameters of our proposed framework are summarized in Table II. Note that we use ‘VehicleThrustSetpoint’ and ‘VehicleTorqueSetpoint’ as control inputs \mathbf{u} to set the thrust and torque (FRD⁴) in Pixhawk 4.

As shown in Algorithm 1, the agent is rewarded at each time step unit, i.e., $1/16$ (s), by following Equation 12 whilst being penalized +1 at each time step unit, according to the constraints: (i) $(\mathbf{x}_t, \mathbf{u}_t) \notin \mathbb{Z}$, specifically $(0, 0, 0) \leq \mathbf{x}_{t,(X,Y,Z)} \leq (6.0, 5.5, 2.0)$ (m), $0 \leq \mathbf{u}_t \leq 12$ (ms^{-1}) in our experiments; and (ii) drifting into the unsafe areas shown in Fig. 2 under external disturbances.

Simulation Training: our constrained simulation scenario is shown in Fig. 2, where each episode has $T = 200$. The reason for this setting is based on *Theorem 2*: if let the episode length be $T = \Theta(\xi^{-2}) = 200$, then there exist $\text{CONV}_{T=200} = 1 - \frac{\mathcal{J}_r(\pi^*) - \mathbb{E}[\mathcal{J}_r(\pi_{out})]}{\mathcal{J}_r(\pi^*) - \mathbb{E}[\mathcal{J}_r(\pi_0)]} \geq 1 - \frac{\xi}{\xi_0} = 1 - \frac{\Theta(\frac{1}{(1-\gamma)\sqrt{T}})}{\Theta(\frac{1}{(1-\gamma)\sqrt{1}})} \approx 93\%$. Thus we can guarantee at least 93% convergence by setting the episode length $T = 200$. The flight task in simulation is to track the seven reference waypoints. In the external disturbance zone, the quadrotor system operates with aerodynamic effects in the horizontal plane in the range $[-3, 3]$ (ms^{-2}).

Real-world Training: Three scenarios are trained in the real physical world⁵: trajectory tracking under external forces (i.e., winds generated from two fans) without obstacles (Flight Tasks 1-2 shown in Fig. 5), trajectory tracking around the static (no external forces) but dense obstacles (Flight Tasks 3-4 shown in Fig. 6) and trajectory tracking under external forces

⁴FRD: coordinate system follows the right-hand rule, where the X-axis points toward the vehicle’s Front, the Y-axis points Right, and the Z-axis points Down.

⁵Video figures in support are available: <https://github.com/Alex-yanranwang/ConsDRED-SMPC>.

TABLE III: Technical Specification of Hardware

No.	Component	Specific Model
1	Frame	QAV250
2	Sensor - Depth Camera	Intel Realsense D435i
3	Sensor - Down-view Rangefinder	Holybro ST VL53L1X
4	Flight Controller	Pixhawk 4
5	Motors	T-Motor F60 Pro IV 1750KV
6	Electronic Speed Controller	BLHeli-32bit 45A 3-6s
7	On-board Companion Computer	DJI Manifold 2-c (CPU Model: Intel Core i7-8550U)
8	Mounts	3D Print for Sensors/ Computer/Controller/Battery

around dense obstacles (Flight Task 5-6 shown in Fig. 7). The magnitude of the external forces (i.e., winds) is in the range $[0, 2.5]$ (ms^{-1}), where the winds are generated from the fans in Scenario 1 and 3.

The hardware specification can be found in Table III. In our setup, we integrate a loop detection process into VID-Fusion [16], following the methodology outlined in [81], to enhance measurement accuracy. This leads to a significant reduction of 14.3% in tracking error, improving the measurement accuracy a range of $[0.010, 0.021]$ (m).

Each flight task is under surveillance from different perspectives, which are an external camera, 3D occupancy grid map constructed based on [82], and an on-board camera (i.e., Intel Realsense D435i). The measured trajectories are also shown from top, front and left perspectives. Compared with the simulated training shown in Fig. 2, the real-world training is more efficiently for ConsDRED (i.e., the disturbance estimator) and can learn directly from the real aerodynamic effects, including a combination of the individual propellers and airframe [29], turbulent effects caused by rotor-rotor and rotor-airframe interactions [30], and other turbulences such as rotor-obstacle interactions [31].

Convergence Performance in Training: the learning curves are displayed in Fig. 3, where we show the training performance of CRPO [12], QuaDRED [23] and our proposed ConsDRED. The performance shows that, in Fig. 3 (a), although all the three algorithms converge to a long-term return eventually, the two distributional approaches, ConsDRED and QuaDRED, outperform the CRL approach, CRPO. QuaDRED achieves the best accumulated rewards, however, the unconstrained QuaDRED does not satisfy the constraint limit in Fig. 3 (b).

For the practical implementation of ConsDRED, we experiment with robustness with regard to the hyperparameter settings. The existing primal-dual approaches such as RCPO [52], CPPPO [53] and PPO [54] are very sensitive to the hyperparameters. Thus additional costs incurred for hyperparameter tuning are inefficient for practical implementation and can hinder important applications, including real-world robots with high uncertainties. Setting the tolerance τ_c variably as $\{0.5, 1, 5, 10, 15\}$, Fig. 4 demonstrates that ConsDRED’s convergence is robust with respect to the tolerance τ_c over the whole training process. Therefore, we can conclude that the tolerance τ_c will not incur large tuning cost when ConsDRED is being implemented.

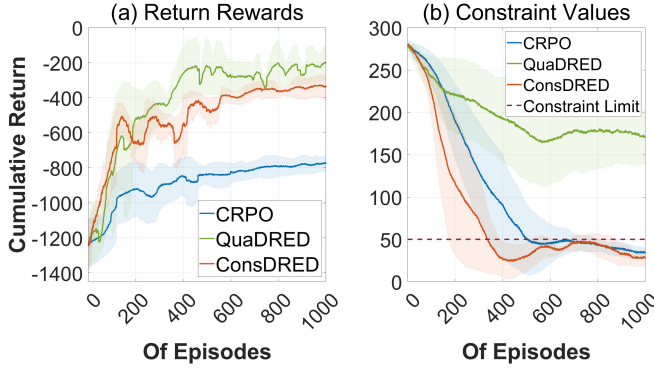


Fig. 3: Learning curves of three RL algorithm: CRPO [12], QuaDRED [23] and ConsDRED. The simulated speed is set as 0.6.

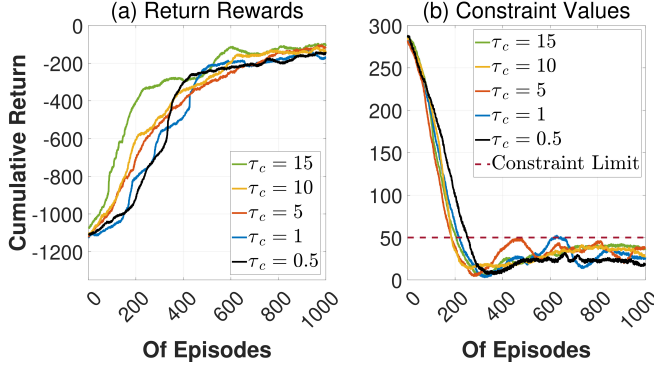


Fig. 4: The robustness of different hyperparameters - i.e., the tolerance τ_c setting - to the reward and constraint convergence process.

B. Comparative performance of ConsDRED-SMPC under variable aerodynamic effects

Simulated Tracking Performance under Programmatic External Forces: we compare our ConsDRED-SMPC against a state-of-the-art trajectory tracking algorithm, GP⁶ [3]-SMPC, and interactive approaches, CRPO [12] and QuaDRED [23], with variable aerodynamic forces added to our simulated environment to evaluate the over-fitting problems of RL. The experiments are based on the trained ConsDRED model described in Section VI-A. We first set the aerodynamic forces as $[0.0, 3.0, 0.0] (m.s^{-2})$. In Fig. 8 and Fig. 9, the tracking position errors and control inputs are depicted for two opposite heading aerodynamic forces (both having the same force $[0.0, 3.0, 0.0] (m.s^{-2})$). Notably, our proposed ConsDRED-SMPC demonstrates the smallest tracking position error and exhibits efficient response to sudden aerodynamic effects in these specific scenarios.

Then two larger and more complex forces, i.e., $[-3.0, 3.0, 0.0]$ and $[-4.0, 4.0, 0.0] (m.s^{-2})$, are used in the scenario shown in Fig. 2. To achieve more accurate outcomes, the number of experiments in Table IV is elevated from 60 to 80 in the second and third instances. To comprehensively

⁶Followed by the baseline [3], we gathered a dataset comprising velocities $[-12, 12] (m.s^{-1})$ to train the GP. This dataset is obtained by tracking randomly generated aggressive trajectories, as shown in Fig. 2.

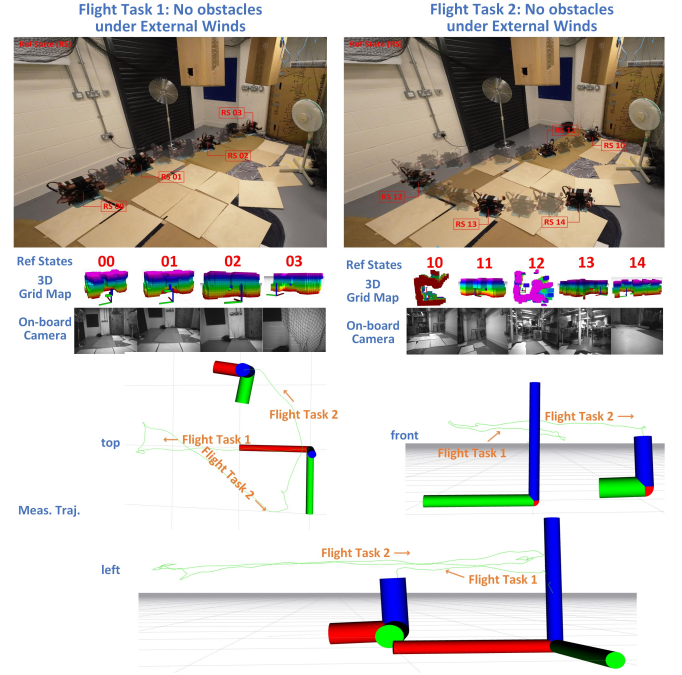


Fig. 5: Real-world Scenario 1: tracking trajectories under external forces without obstacles, where the agent learns the aerodynamic effects like turbulent effects caused by dynamic rotor-rotor and rotor-airframe interactions [29] in Flight Task 1-2.

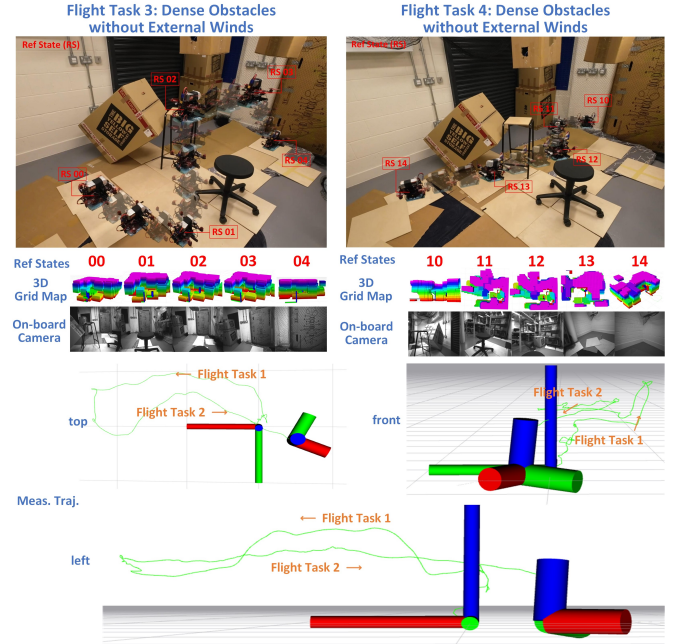


Fig. 6: Real-world Scenario 2: tracking trajectories around the static (no external forces) but dense obstacles, where the agent learns the turbulent effects from rotor-obstacle interactions [31] in Flight Task 3-4.

assess the performance, we conduct a thorough comparison in Table IV, involving various controllers: ‘PD [83]’ (a

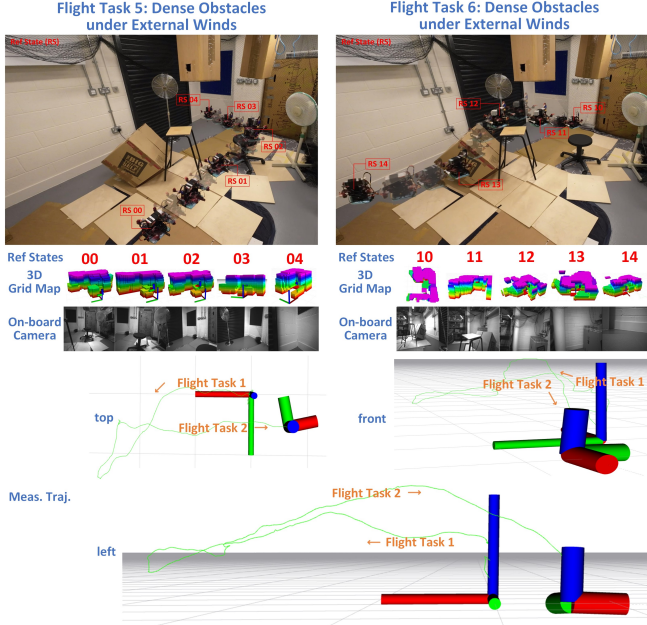


Fig. 7: Real-world Scenario 3: tracking trajectories under external forces around dense obstacles, where the agent learns the comprehensive aerodynamic effects from a combination of dynamic rotor-rotor, rotor-airframe, and rotor-obstacle interactions in Flight Task 5-6.

standard controller⁷), ‘PD + VID-Fusion [16]’ (a standard adaptive controller), ‘ADP [27]’ (a combination of dynamic programming and RL⁸), ‘SMPC’ (a baseline controller), ‘SMPC + VID-Fusion’ (a combination of a baseline controller and an adaptive estimator), ‘GP-SMPC’ (a combination of GP [3] and SMPC), ‘CRPO + SMPC’ (a combination of CRPO [12] and SMPC), ‘QuaDRED-SMPC’ (a combination of QuaDRED [23], DDPG [9], and SMPC), and ‘ConsDRED-SMPC’ (our proposed method). Analyzing the outcomes in TABLE IV, it becomes evident that the adaptive controller ‘PD + VID-Fusion’ performs poorly. This is primarily attributed to the inherent limitations of the vision-inertial measurement module in VID-Fusion [16], leading to inaccurate estimations, especially in larger aerodynamics. To address this issue, a disturbance estimator such as ConsDRED and QuaDRED [23] is introduced into the control framework, as depicted in Fig. 1. Further insights from the results in TABLE IV reveal that ‘PD’ and ‘PD + VID-Fusion’ exhibit poor performance. Consequently, we exclude these for real-world experiments shown in TABLE V.

Our results also show that interactive approaches are not always greater than non-interactive approaches. For example, ‘CRPO + SMPC’ has a lower success⁹ times than GP-SMPC, whilst there is little difference in the operation time and

⁷We tune parameters by initially employing manual tuning and subsequently performing auto-tuning, as outlined in [84], within the PX4 user guide [85].

⁸The parameter setting is derived from [27], wherein the optimal parameters are dynamically learned online based on the quadrotor state.

⁹A successful flight: the quadrotor completes the flight from the starting point to the destination point, allowing for minor collisions without resulting in a collapse.

TABLE IV: Simulated trajectory tracking under programmatic external forces, where the three external forces are: $E_{f,1} = [0.0, 3.0, 0.0] (ms^{-2})$, $E_{f,2} = [-3.0, 3.0, 0.0] (ms^{-2})$ and $E_{f,3} = [-4.0, 4.0, 0.0] (ms^{-2})$.

Ex. forces	Method	Succ. Times	Time (s)	Accum. Err. (m)	RMSE (m)	Cons. Return
$E_{f,1}$	PD [83]	7/60	37.61	31.53	1.31	252
	PD + VID-Fusion [16]	25/60	29.16	25.51	0.94	239
	ADP [27]	21/60	33.87	29.43	0.95	246
	SMPC [23]	29/60	32.16	25.48	0.86	251
	SMPC + VID-Fusion	47/60	17.31	12.59	0.48	247
	GP [3]-SMPC	41/60	26.85	21.62	0.62	231
	CRPO [12] + SMPC	41/60	31.26	19.58	0.58	36
	QuaDRED-SMPC [23]	55/60	10.58	7.53	0.21	141
	ConsDRED-SMPC	53/60	10.89	5.52	0.16	18
$E_{f,2}$	PD	2/80	-	-	-	-
	PD + VID-Fusion	10/80	38.09	29.28	1.17	255
	ADP	15/80	41.16	32.56	1.51	259
	SMPC	9/80	40.67	31.74	1.33	242
	SMPC + VID-Fusion	56/80	23.84	13.83	0.50	246
	GP-SMPC	15/80	36.15	24.11	0.87	273
	CRPO + SMPC	50/80	28.33	19.84	0.67	31
	QuaDRED-SMPC	66/80	12.20	9.35	0.23	176
	ConsDRED-SMPC	67/80	14.11	9.89	0.26	33
$E_{f,3}$	PD	0/80	-	-	-	-
	PD + VID-Fusion	2/80	-	-	-	-
	ADP	8/80	42.26	39.64	1.77	257
	SMPC	2/80	-	-	-	-
	SMPC + VID-Fusion	48/80	30.62	24.07	0.84	250
	GP-SMPC	0/80	-	-	-	-
	CRPO + SMPC	41/80	28.56	29.11	0.97	35
	QuaDRED-SMPC	67/80	13.62	12.36	0.34	189
	ConsDRED-SMPC	69/80	11.87	11.98	0.31	40

accumulative tracking error with relatively small aerodynamic forces. However, compared with GP-SMPC, our proposed ConsDRED-SMPC achieves improvements of $> 61\%$ in operation time, $> 70\%$ in RMSE¹⁰ tracking errors, and $> 87\%$ in accumulative constrained returns, respectively. Intuitively, the superior performance of both distributional RL and SMPC over their conventional counterparts stems from their more comprehensive and enriched representations — i.e., the entire value distribution in distributional RL and probabilistic descriptions in SMPC. These approaches help avoid the worst-case conservatism. The two distributional RL approaches, i.e., ‘QuaDRED-SMPC’ and ‘ConsDRED-SMPC’, have closed success times, operation time and tracking errors, where ‘QuaDRED-SMPC’ has better performance in some cases. However, compared to ‘QuaDRED-SMPC’, our ‘ConsDRED-SMPC’ achieves 87.2%, 81.3% and 78.8% improvements in constrained returns.

The simulated results highlight a significant portion of the performance improvement arising from the integration of a wind estimator (VID-Fusion). This integration leads to a 23% improvement in relatively small wind conditions and a substantial 46% improvement in larger wind conditions. Moreover, the trend indicates that the contribution of ConsDRED to performance becomes more pronounced with increasing external wind intensity, escalating from 54% to 77%.

¹⁰The RMSE metric in both Table IV and Table V represents the average RMSE over all successful trajectories for a specific controller, not a single trajectory.

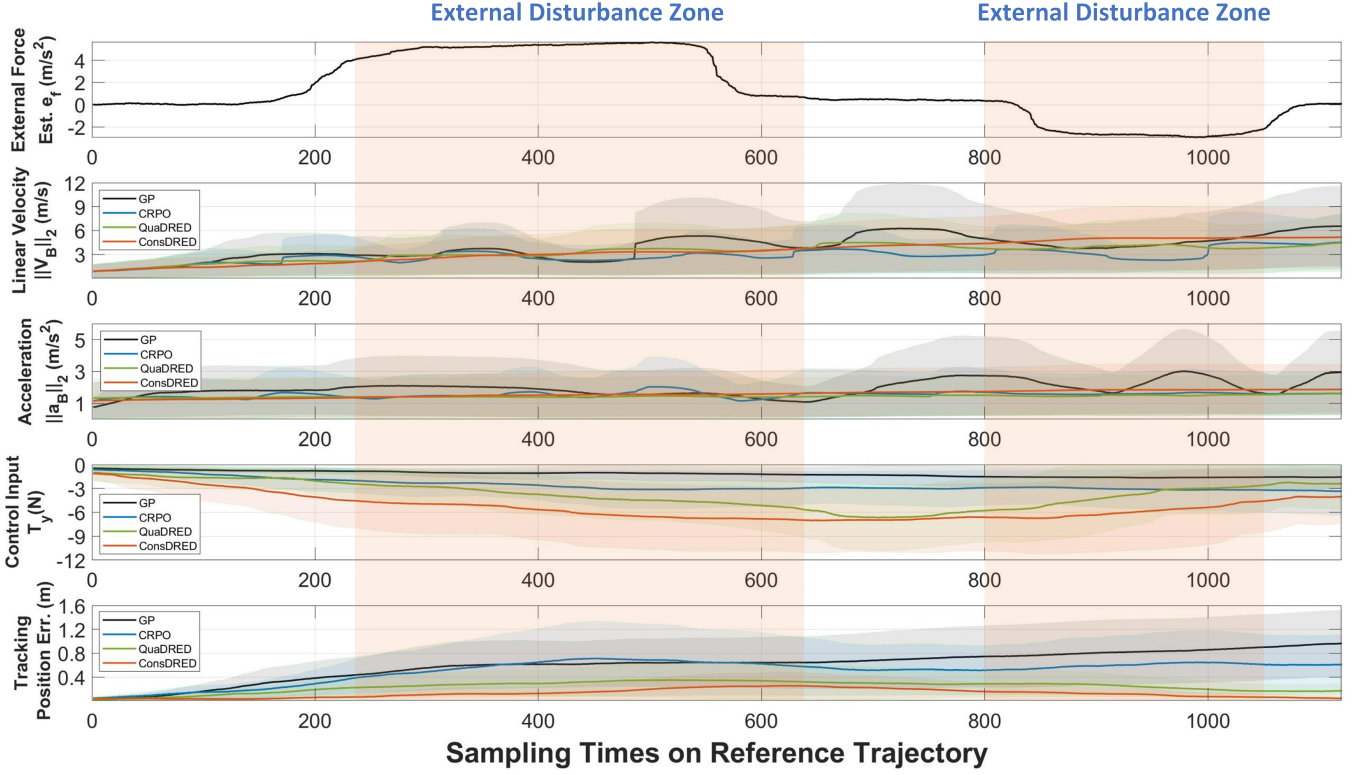


Fig. 8: Simulation tracking performance assessed with variance measurement: the external force estimation $e_f(m/s^2)$, linear velocity $\|V_B\|_2$, acceleration $\|a_B\|_2$, the control input T_y (expressed in the body frame) and tracking position error (m). The X-axis unit corresponds to the number of sampling times, with 1100 sampling points evenly distributed along a trajectory. The results from a single run are depicted in Fig. 9.

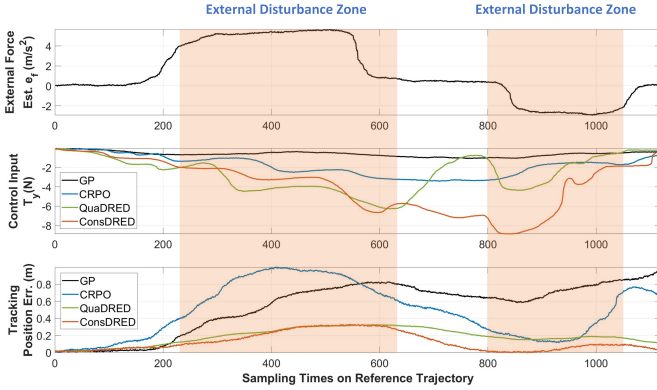


Fig. 9: Simulation result from one run: the external force estimation e_f , the control input T_y (expressed in the body frame), and tracking position error (m).

Real-world Tracking Performance under Variable Disturbances: The aim is to evaluate two properties of the trained ConsDRED: 1) convergence quality in the real physical experiments, and 2) generalization capability under unprecedented external forces.

We firstly evaluate the convergence quality in Scenario 3 (shown in Fig. 7). The external forces from the left / right fans are represented as $\{F1_{l,s3}, F1_{r,s3}\}$, both of which are within training range, $[0, 2.5] (ms^{-1})$ generated from fans.

TABLE V: Real-world trajectory tracking under variable external forces: the scenario 1 (shown in Fig. 5) and 3 (shown in Fig. 7) are applied for tracking performance evaluation. Let the external forces from the left / right fans in scenario 1 / 3 be $F1_{l,s3} = 2.5 (ms^{-1})$, $F1_{r,s3} = 1.5 (ms^{-1})$; $F2_{l,s1} = 3.5 (ms^{-1})$, $F2_{r,s1} = 2.5 (ms^{-1})$; and $F3_{l,s3} = 3.5 (ms^{-1})$, $F3_{r,s3} = 2.5 (ms^{-1})$.

Ex. forces	Method	Succ. Times	Time (s)	Accum. Err. (m)	RMSE (m)	Cons. Return
$F1_{l,s3}$ $F1_{r,s3}$	SMPC	12/20	17.76	4.12	0.314	239
	SMPC + VID-Fusion	17/20	16.02	1.95	0.120	224
	GP-SMPC	16/20	15.95	3.81	0.303	216
	CRPO + SMPC	14/20	17.09	2.10	0.119	30
	QuaDRED-SMPC	18/20	15.56	1.85	0.103	111
	ConsDRED-SMPC	18/20	15.91	1.91	0.106	33
$F2_{l,s1}$ $F2_{r,s1}$	SMPC	2/20	18.52	5.13	0.572	249
	SMPC + VID-Fusion	13/20	17.67	2.68	0.301	245
	GP-SMPC	7/20	17.20	3.58	0.302	210
	CRPO + SMPC	13/20	17.41	2.08	0.151	32
	QuaDRED-SMPC	20/20	16.35	1.65	0.102	97
	ConsDRED-SMPC	20/20	16.52	1.71	0.102	18
$F3_{l,s3}$ $F3_{r,s3}$	SMPC	0/30	-	-	-	-
	SMPC + VID-Fusion	7/30	18.03	3.71	0.296	237
	GP-SMPC	2/30	18.52	4.83	0.534	238
	CRPO + SMPC	6/30	17.52	3.52	0.276	41
	QuaDRED-SMPC	25/30	16.12	2.82	0.192	156
	ConsDRED-SMPC	28/30	15.98	2.06	0.109	41

We only change the obstacle positions slightly and keep the same number and similar density of obstacles. The quadrotor

is required to perform the flight task described in Fig. 7, where the reference trajectories are generated by Kino-JSS [5]. The generalization capability is next evaluated in Scenario 1 and 3, where the feeding external forces are unprecedented, i.e., out of the range $[0, 2.5] (ms^{-1})$. $\{\mathbf{F2}_{l,s1}, \mathbf{F2}_{r,s1}\}$ and $\{\mathbf{F3}_{l,s3}, \mathbf{F3}_{r,s3}\}$ denotes the external forces from the left / right fans shown in Fig. 5 and Fig. 7, respectively.

The first case in Table V shows again in real flight tasks that compared with ‘SMPC + VID-Fusion’, RL-based approaches are not always significantly better, especially under relatively small external disturbances, which verifies empirically the conclusion in [3], [23]. In terms of the convergence quality, although all approaches can complete the tasks in most instances, the two distributional RL approaches significantly outperform ‘SMPC’, ‘GP¹¹-SMPC’ and ‘CRPO + SMPC’. Then the second and third cases show good generalization ability of the proposed ‘ConsDRED-SMPC’, which achieves comprehensively improved results in operation time, accumulative tracking errors and constrained returns. Since ‘GP-SMPC’ and ‘CRPO + SMPC’ have low ‘Success Times’ (< 4 in the first 20 experiments), to obtain more accurate value, the experimental number in Table V increases from 20 to 30 in the third case.

Compared with the two interactive RL approaches, i.e., constrained ‘CRPO + SMPC’ and the unconstrained ‘QuaDRED-SMPC’, we also find that ConsDRED-SMPC balances a tradeoff between pursuing higher performance and obeying safety constraints: (i) ‘QuaDRED’ outperforms our proposed ‘ConsDRED’ in some cases, but it does not consider the constraints for safety taking an unconstrained approach; and ii) ‘CRPO’ behaves as safely as ‘ConsDRED’ (‘Cons. Return’ in Table V), however, it performs poorly on the success times, operation time and tracking errors, because of its conservative decisions.

The influence of ConsDRED becomes even more evident in this real-world tracking experiments, shown in TABLE V. The contribution of ConsDRED rises significantly from 6.7% to 57% as the wind intensifies, transitioning from $\mathbf{F1}_{l,s3} = 2.5 (ms^{-1})$, $\mathbf{F1}_{r,s3} = 1.5 (ms^{-1})$ to $\mathbf{F2}_{l,s1} = 3.5 (ms^{-1})$, $\mathbf{F2}_{r,s1} = 2.5 (ms^{-1})$.

VII. CONCLUSION

We propose ConsDRED-SMPC, an accurate trajectory tracking framework for quadrotors operating in environments with variable aerodynamic forces. ConsDRED-SMPC combines aerodynamic disturbance estimation and stochastic optimal control to address the aerodynamic effects on quadrotor tracking. A constrained distributional RL with quantile approximation, ConsDRED, is developed to improve the accuracy of aerodynamic effect estimation, where it achieves an $\Theta(1/\sqrt{T})$ convergence rate to the global optimum whilst an $\Theta(1/m^{\frac{H}{4}})$ approximation error. Using SADP for control parameterization to guarantee convexity, a SMPC is used to avoid conservative control returns and significantly improves

the accuracy of quadrotor tracking. The aerodynamic disturbances are considered to have non-zero mean in the entire ConsDRED-SMPC framework. For practical implementation, firstly we empirically demonstrate ConsDRED’s convergence for training in simulation before moving to real-world training and validation. In contrast to most existing CRL approaches, our proposed ConsDRED is less sensitive to the tolerance τ_c setting, i.e., hyperparameter tuning, and is hence easier to tune. Finally, we demonstrate that, in both simulated and real-world experiments, our proposed approach can track aggressive trajectories accurately under complex aerodynamic effects, while guaranteeing both the convergence of ConsDRED and the stability of the whole control framework.

Our ongoing work concerns demonstrating the concept of recursive feasibility in SMPC, and future work will involve additional data collection and training processes in the wind tunnel to precisely identify the turbulent effects. We also prioritize investigating outdoor environments with additional unknowns and complexities. To reduce the computational complexity, we will implement ConsDRED-SMPC on dedicated hardware, for example, via FPGA implementation.

REFERENCES

- [1] Balmukund Mishra, Deepak Garg, Pratik Narang, and Vipul Mishra. Drone-surveillance for search and rescue in natural disaster. *Computer Communications*, 156:1–10, 2020.
- [2] Didula Dissanayaka, Thumeera R Wanasinghe, Oscar De Silva, Awantha Jayasiri, and George KI Mann. Review of navigation methods for uav-based parcel delivery. *IEEE Transactions on Automation Science and Engineering*, 2023.
- [3] Guillem Torrente, Elia Kaufmann, Philipp Föhn, and Davide Scaramuzza. Data-driven mpc for quadrotors. *IEEE Robotics and Automation Letters*, 6(2):3769–3776, 2021.
- [4] Matthias Faessler, Antonio Franchi, and Davide Scaramuzza. Differential flatness of quadrotor dynamics subject to rotor drag for accurate tracking of high-speed trajectories. *IEEE Robotics and Automation Letters*, 3(2):620–626, 2017.
- [5] Yanran Wang, James O’Keefe, Qiuchen Qian, and David Boyle. Kinojrm: A framework for efficient and accurate quadrotor trajectory generation and tracking in dynamic environments. In *2022 International Conference on Robotics and Automation (ICRA)*, pages 11036–11043. IEEE, 2022.
- [6] Nathan A Spielberg, Matthew Brown, and J Christian Gerdes. Neural network model predictive motion control applied to automated driving with unknown friction. *IEEE Transactions on Control Systems Technology*, 2021.
- [7] Fei Dong, Xingchen Li, Keyou You, and Shiji Song. Deep neural network based model predictive control for standoff tracking by a quadrotor uav. In *2022 IEEE 61st Conference on Decision and Control (CDC)*, pages 1810–1815. IEEE, 2022.
- [8] Qingrui Zhang, Wei Pan, and Vasso Repa. Model-reference reinforcement learning for collision-free tracking control of autonomous surface vehicles. *IEEE Transactions on Intelligent Transportation Systems*, 2021.
- [9] Timothy P Lillicrap, Jonathan J Hunt, Alexander Pritzel, Nicolas Heess, Tom Erez, Yuval Tassa, David Silver, and Daan Wierstra. Continuous control with deep reinforcement learning. *arXiv preprint arXiv:1509.02971*, 2015.
- [10] Alan W Beggs. On the convergence of reinforcement learning. *Journal of economic theory*, 122(1):1–36, 2005.
- [11] Javier Garcia and Fernando Fernández. A comprehensive survey on safe reinforcement learning. *Journal of Machine Learning Research*, 16(1):1437–1480, 2015.
- [12] Tengyu Xu, Yingbin Liang, and Guanghui Lan. Crpo: A new approach for safe reinforcement learning with convergence guarantee. In *International Conference on Machine Learning*, pages 11480–11491. PMLR, 2021.

¹¹To fit the GPs, flight data from the real world is collected, as detailed in Section III-F in [3], and visualized in the accompanying video ⁵.

- [13] Nicolai A Lynnerup, Laura Nolling, Rasmus Hasle, and John Hallam. A survey on reproducibility by evaluating deep reinforcement learning algorithms on real-world robots. In *Conference on Robot Learning*, pages 466–489. PMLR, 2020.
- [14] Huan Nguyen, Mina Kamel, Kostas Alexis, and Roland Siegwart. Model predictive control for micro aerial vehicles: A survey. In *2021 European Control Conference (ECC)*, pages 1556–1563. IEEE, 2021.
- [15] Florian Ostmann and Cosmina Dorobantu. Ai in financial services. *Alan Turing Institute*. doi, 10, 2021.
- [16] Ziming Ding, Tiankai Yang, Kunyi Zhang, Chao Xu, and Fei Gao. Vid-fusion: Robust visual-inertial-dynamics odometry for accurate external force estimation. *arXiv preprint arXiv:2011.03993*, 2020.
- [17] Will Dabney, Mark Rowland, Marc Bellemare, and Rémi Munos. Distributional reinforcement learning with quantile regression. In *Proceedings of the AAAI Conference on Artificial Intelligence*, volume 32, 2018.
- [18] Shangdong Zhang and Hengshuai Yao. Quota: The quantile option architecture for reinforcement learning. In *Proceedings of the AAAI Conference on Artificial Intelligence*, volume 33, pages 5797–5804, 2019.
- [19] Jingyu Zhang and Toshiyuki Ohtsuka. Stochastic model predictive control using simplified affine disturbance feedback for chance-constrained systems. In *2021 American Control Conference (ACC)*, pages 1256–1261. IEEE, 2021.
- [20] Johan Lofberg. Approximations of closed-loop minimax mpc. In *42nd IEEE International Conference on Decision and Control (IEEE Cat. No. 03CH37475)*, volume 2, pages 1438–1442. IEEE, 2003.
- [21] Zhong-Ping Jiang and Yuan Wang. Input-to-state stability for discrete-time nonlinear systems. *Automatica*, 37(6):857–869, 2001.
- [22] Ludovic Rifford. Existence of lipschitz and semiconcave control-lyapunov functions. *SIAM Journal on Control and Optimization*, 39(4):1043–1064, 2000.
- [23] Yanran Wang, James O’Keeffe, Qiuchen Qian, and David Boyle. Interpretable stochastic model predictive control using distributional reinforced estimation for quadrotor tracking systems. In *2022 IEEE 61st Conference on Decision and Control (CDC)*, pages 3335–3342. IEEE, 2022.
- [24] Samer Abdelmoeti and Raffaella Carloni. Robust control of uavs using the parameter space approach. In *2016 IEEE/RSJ International Conference on Intelligent Robots and Systems (IROS)*, pages 5632–5637. IEEE, 2016.
- [25] Guilherme V Raffo and Marcelino M de Almeida. Nonlinear robust control of a quadrotor uav for load transportation with swing improvement. In *2016 American control conference (ACC)*, pages 3156–3162. IEEE, 2016.
- [26] Qingrui Zhang and Hugh HT Liu. Aerodynamic model-based robust adaptive control for close formation flight. *Aerospace Science and Technology*, 79:5–16, 2018.
- [27] Liqian Dou, Xiaotong Su, Xinyi Zhao, Qun Zong, and Lei He. Robust tracking control of quadrotor via on-policy adaptive dynamic programming. *International Journal of Robust and Nonlinear Control*, 31(7):2509–2525, 2021.
- [28] John J Bertin and Russell M Cummings. *Aerodynamics for engineers*. Cambridge University Press, 2021.
- [29] Gabriel Hoffmann, Haomiao Huang, Steven Waslander, and Claire Tomlin. Quadrotor helicopter flight dynamics and control: Theory and experiment. In *AIAA guidance, navigation and control conference and exhibit*, page 6461, 2007.
- [30] Carl R Russell, Jaewoo Jung, Gina Willink, and Brett Glasner. Wind tunnel and hover performance test results for multicopter uas vehicles. In *American Helicopter Society (AHS) International Annual Forum and Technology Display*, number ARC-E-DAA-TN31096, 2016.
- [31] Derya Kaya and Ali T Kutay. Aerodynamic modeling and parameter estimation of a quadrotor helicopter. In *AIAA Atmospheric Flight Mechanics Conference*, page 2558, 2014.
- [32] Ezra Tal and Sertac Karaman. Accurate tracking of aggressive quadrotor trajectories using incremental nonlinear dynamic inversion and differential flatness. *IEEE Transactions on Control Systems Technology*, 29(3):1203–1218, 2020.
- [33] Seung Jae Lee, Seung Hyun Kim, and Hyoun Jin Kim. Robust translational force control of multi-rotor uav for precise acceleration tracking. *IEEE Transactions on Automation Science and Engineering*, 17(2):562–573, 2019.
- [34] Davide Bicego, Jacopo Mazzetto, Ruggero Carli, Marcello Farina, and Antonio Franchi. Nonlinear model predictive control with enhanced actuator model for multi-rotor aerial vehicles with generic designs. *Journal of Intelligent & Robotic Systems*, 100(3):1213–1247, 2020.
- [35] Alessandro Saviolo and Giuseppe Loianno. Learning quadrotor dynamics for precise, safe, and agile flight control. *Annual Reviews in Control*, 2023.
- [36] Antonio Loquercio, Elia Kaufmann, René Ranftl, Matthias Müller, Vladlen Koltun, and Davide Scaramuzza. Learning high-speed flight in the wild. *Science Robotics*, 6(59):eabg5810, 2021.
- [37] Rupam Singh and Bharat Bhushan. Evolving intelligent system for trajectory tracking of unmanned aerial vehicles. *IEEE Transactions on Automation Science and Engineering*, 19(3):1971–1984, 2021.
- [38] Ying Wu, Mou Chen, Hongyi Li, and Mohammed Chadli. Event-triggered-based adaptive nn cooperative control of six-rotor uavs with finite-time prescribed performance. *IEEE Transactions on Automation Science and Engineering*, 2023.
- [39] Carlo Rizzardo, Fei Chen, and Darwin Caldwell. Sim-to-real via latent prediction: Transferring visual non-prehensile manipulation policies. *Frontiers in Robotics and AI*, 9:1067502, 2023.
- [40] Chaojie Zhu, Jicheng Chen, Makoto Iwasaki, and Hui Zhang. Event-triggered deep learning control of quadrotors for trajectory tracking. *IEEE Transactions on Industrial Electronics*, 2023.
- [41] Fabio Muratore, Fabio Ramos, Greg Turk, Wenhao Yu, Michael Gienger, and Jan Peters. Robot learning from randomized simulations: A review. *Frontiers in Robotics and AI*, page 31, 2022.
- [42] Sebastian Höfer, Kostas Bekris, Ankur Handa, Juan Camilo Gamboa, Melissa Mozifian, Florian Golemo, Chris Atkeson, Dieter Fox, Ken Goldberg, John Leonard, et al. Sim2real in robotics and automation: Applications and challenges. *IEEE transactions on automation science and engineering*, 18(2):398–400, 2021.
- [43] Alessandro Saviolo, Guanrui Li, and Giuseppe Loianno. Physics-inspired temporal learning of quadrotor dynamics for accurate model predictive trajectory tracking. *IEEE Robotics and Automation Letters*, 7(4):10256–10263, 2022.
- [44] Gabriele Tiboni, Karol Arndt, and Ville Kyrki. Dropo: Sim-to-real transfer with offline domain randomization. *Robotics and Autonomous Systems*, 166:104432, 2023.
- [45] Dániel Horváth, Gábor Erdős, Zoltán Istenes, Tomáš Horváth, and Sándor Földi. Object detection using sim2real domain randomization for robotic applications. *IEEE Transactions on Robotics*, 39(2):1225–1243, 2022.
- [46] Yecheng Ma, Dinesh Jayaraman, and Osbert Bastani. Conservative offline distributional reinforcement learning. *Advances in Neural Information Processing Systems*, 34, 2021.
- [47] Marc G Bellemare, Will Dabney, and Rémi Munos. A distributional perspective on reinforcement learning. In *International Conference on Machine Learning*, pages 449–458. PMLR, 2017.
- [48] Matteo Hessel, Joseph Modayil, Hado Van Hasselt, Tom Schaul, Georg Ostrovski, Will Dabney, Dan Horgan, Bilal Piot, Mohammad Azar, and David Silver. Rainbow: Combining improvements in deep reinforcement learning. In *Thirty-second AAAI conference on artificial intelligence*, 2018.
- [49] Mark Rowland, Robert Dadashi, Saurabh Kumar, Rémi Munos, Marc G Bellemare, and Will Dabney. Statistics and samples in distributional reinforcement learning. In *International Conference on Machine Learning*, pages 5528–5536. PMLR, 2019.
- [50] Thanh Tang Nguyen, Sunil Gupta, and Svetha Venkatesh. Distributional reinforcement learning via moment matching. In *Proceedings of the AAAI Conference on Artificial Intelligence (AAAI)*, 2021.
- [51] Shangding Gu, Long Yang, Yali Du, Guang Chen, Florian Walter, Jun Wang, Yaodong Yang, and Alois Knoll. A review of safe reinforcement learning: Methods, theory and applications. *arXiv preprint arXiv:2205.10330*, 2022.
- [52] Chen Tessler, Daniel J Mankowitz, and Shie Mannor. Reward constrained policy optimization. *arXiv preprint arXiv:1805.11074*, 2018.
- [53] Adam Stooke, Joshua Achiam, and Pieter Abbeel. Responsive safety in reinforcement learning by pid lagrangian methods. In *International Conference on Machine Learning*, pages 9133–9143. PMLR, 2020.
- [54] Dongsheng Ding, Xiaohan Wei, Zhuoran Yang, Zhaoran Wang, and Mihailo Jovanovic. Provably efficient safe exploration via primal-dual policy optimization. In *International Conference on Artificial Intelligence and Statistics*, pages 3304–3312. PMLR, 2021.
- [55] Yinlam Chow, Ofir Nachum, Edgar Duenez-Guzman, and Mohammad Ghavamzadeh. A lyapunov-based approach to safe reinforcement learning. *Advances in neural information processing systems*, 31, 2018.
- [56] Yongshuai Liu, Jiaxin Ding, and Xin Liu. Ipo: Interior-point policy optimization under constraints. In *Proceedings of the AAAI Conference on Artificial Intelligence*, volume 34, pages 4940–4947, 2020.
- [57] Qinglai Wei, Zesheng Yang, Huaizhong Su, and Lijian Wang. Online adaptive dynamic programming for optimal self-learning control of vtol

- aircraft systems with disturbances. *IEEE Transactions on Automation Science and Engineering*, 2022.
- [58] Kemin Zhou and John Comstock Doyle. *Essentials of robust control*, volume 104. Prentice hall Upper Saddle River, NJ, 1998.
- [59] David Mayne. Robust and stochastic model predictive control: Are we going in the right direction? *Annual Reviews in Control*, 41:184–192, 2016.
- [60] Ali Mesbah. Stochastic model predictive control: An overview and perspectives for future research. *IEEE Control Systems Magazine*, 36(6):30–44, 2016.
- [61] Sihao Sun, Angel Romero, Philipp Foehn, Elia Kaufmann, and Davide Scaramuzza. A comparative study of nonlinear mpc and differential-flatness-based control for quadrotor agile flight. *IEEE Transactions on Robotics*, 38(6):3357–3373, 2022.
- [62] Alexander T Schwarm and Michael Nikolaou. Chance-constrained model predictive control. *AIChE Journal*, 45(8):1743–1752, 1999.
- [63] Chrystian Pool Edmundo Yuca Huanca, Gian Paolo Incremona, and Patrizio Colaneri. Design of a distributed switching model predictive control for quadrotor uavs aggregation. *IEEE Control Systems Letters*, 2023.
- [64] James A Primbs and Chang Hwan Sung. Stochastic receding horizon control of constrained linear systems with state and control multiplicative noise. *IEEE transactions on Automatic Control*, 54(2):221–230, 2009.
- [65] Diego Munoz-Carpintero and Mark Cannon. Convergence of stochastic nonlinear systems and implications for stochastic model-predictive control. *IEEE Transactions on Automatic Control*, 66(6):2832–2839, 2020.
- [66] Paul J Goulart and Eric C Kerrigan. Input-to-state stability of robust receding horizon control with an expected value cost. *Automatica*, 44(4):1171–1174, 2008.
- [67] Joel AE Andersson, Joris Gillis, Greg Horn, James B Rawlings, and Moritz Diehl. Casadi: a software framework for nonlinear optimization and optimal control. *Mathematical Programming Computation*, 11(1):1–36, 2019.
- [68] Eitan Altman. *Constrained Markov decision processes: stochastic modeling*. Routledge, 1999.
- [69] Marc G Bellemare, Will Dabney, and Mark Rowland. *Distributional reinforcement learning*. MIT Press, 2023.
- [70] Yunhao Tang, Mark Rowland, Rémi Munos, Bernardo Ávila Pires, Will Dabney, and Marc G Bellemare. The nature of temporal difference errors in multi-step distributional reinforcement learning. *arXiv preprint arXiv:2207.07570*, 2022.
- [71] Richard S Sutton. Learning to predict by the methods of temporal differences. *Machine learning*, 3(1):9–44, 1988.
- [72] Richard S Sutton and Andrew G Barto. *Reinforcement learning: An introduction*. MIT press, 2018.
- [73] Paul James Goulart. *Affine feedback policies for robust control with constraints*. PhD thesis, University of Cambridge, 2007.
- [74] Robin Verschueren, Gianluca Frison, Dimitris Kouzoupis, Niels van Duijkeren, Andrea Zanelli, Rien Quirynen, and Moritz Diehl. Towards a modular software package for embedded optimization. *IFAC-PapersOnLine*, 51(20):374–380, 2018.
- [75] Qi Cai, Zhuoran Yang, Jason D Lee, and Zhaoran Wang. Neural temporal-difference and q-learning provably converge to global optima. *arXiv preprint arXiv:1905.10027*, 2019.
- [76] Cédric Villani. The wasserstein distances. In *Optimal transport*, pages 93–111. Springer, 2009.
- [77] Philippe Clement and Wolfgang Desch. An elementary proof of the triangle inequality for the wasserstein metric. *Proceedings of the American Mathematical Society*, 136(1):333–339, 2008.
- [78] Ali Rahimi and Benjamin Recht. Weighted sums of random kitchen sinks: Replacing minimization with randomization in learning. *Advances in neural information processing systems*, 21, 2008.
- [79] Sham Kakade and John Langford. Approximately optimal approximate reinforcement learning. In *In Proc. 19th International Conference on Machine Learning*. Citeseer, 2002.
- [80] Fadri Furrer, Michael Burri, Markus Achtelik, and Roland Siegwart. Rotors—a modular gazebo mav simulator framework. In *Robot operating system (ROS)*, pages 595–625. Springer, 2016.
- [81] Tong Qin, Peiliang Li, and Shaojie Shen. Vins-mono: A robust and versatile monocular visual-inertial state estimator. *IEEE Transactions on Robotics*, 34(4):1004–1020, 2018.
- [82] Boyu Zhou, Jie Pan, Fei Gao, and Shaojie Shen. Raptor: Robust and perception-aware trajectory replanning for quadrotor fast flight. *IEEE Transactions on Robotics*, 37(6):1992–2009, 2021.
- [83] Kexin Guo, Wenyu Zhang, Yukai Zhu, Jindou Jia, Xiang Yu, and Youmin Zhang. Safety control for quadrotor uav against ground effect and blade damage. *IEEE Transactions on Industrial Electronics*, 69(12):13373–13383, 2022.
- [84] Khoa Dang Nguyen and Cheolkeun Ha. Development of hardware-in-the-loop simulation based on gazebo and pixhawk for unmanned aerial vehicles. *International Journal of Aeronautical and Space Sciences*, 19:238–249, 2018.
- [85] Lorenz Meier, Dominik Honegger, and Marc Pollefeys. Px4: A node-based multithreaded open source robotics framework for deeply embedded platforms. In *2015 IEEE international conference on robotics and automation (ICRA)*, pages 6235–6240. IEEE, 2015.



Yanran Wang received the M.Sc. degree in Aeronautics and Astronautics Science and Technology at Shanghai Jiao Tong University, Shanghai, China, in 2020, and B.Sc. degree in Automation at Southeast University, Nanjing, China, in 2017. He is currently pursuing the Ph.D. degree at Imperial College London. His research interests mainly include reliable learning-based controller in cyber-physical Systems.



David Boyle (Member, IEEE) is an Associate Professor (Senior Lecturer) with the Dyson School of Design Engineering, Imperial College London. He received the B.Eng. and Ph.D. degrees in Computer and Computer and Electronic Engineering from the University of Limerick, Ireland, in 2005 and 2009, respectively. His research interests include the design of secure, private, and trustworthy cyber-physical systems.